Hybrid Coupler Implemented as a Phase Shifter

John P. Vitale
Marquette University

HYBRID COUPLER IMPLEMENTED AS A PHASE SHIFTER

by

John P. Vitale, B.S.

A Thesis Submitted to the Faculty of the
Graduate School, Marquette University,
in Partial Fulfillment of the Requirements for
the Degree of Master of Science

Milwaukee, Wisconsin

December 2012

ABSTRACT
HYBRID COUPLER IMPLEMENTED AS A PHASE SHIFTER

John P. Vitale, B.S.

Marquette University, 2012

Phase shifters are two-port microwave devices which take an input signal and output a phase shifted version of the signal. These devices can be used in phased antenna arrays, frequency translators, and IQ modulator/demodulator systems. The goal for this work is to construct a hybrid coupler phase shifter which will provide a 90 degree phase shift to a signal with a center frequency of 1800 MHz over a 5% bandwidth.

This work is novel because the hybrid coupler phase shifter has not been extensively studied. Some papers have provided rough guidelines for constructing these shifters, but there is little exploration of performance.

This work uses RF Sim as a simulation tool to provide design analysis, and experimental work was performed in the RF laboratory at the Marquette University College of Engineering.

The basis for the design of the phase shifter comes from idealized design guidelines found in white papers. Realistic effects inherent in the design are shown in the final results. Updated simulation results are provided which provide compensation for these effects to achieve the desired performance.

ACKNOWLEDGMENTS

John P. Vitale, B.S.

There are many people to thank for the completion of the work on this thesis. Many people have provided assistance academically, monetarily and with their motivational support.

I would first like to thank my advisor Dr. James Richie. He has taught me a great deal about EM throughout my collegiate career and during my thesis work. He has also helped me in growing as a researcher and technical writer.

Secondly, I thank participants in the Microwave Seminar who have provided additional insight into technical problems I experienced during this work. I received invaluable information from experienced engineers and peers which helped me to successfully complete this work.

I also thank Marquette University for providing me with a TA grant to help pay for my time working on this degree. Finally, I must thank my family for providing both motivational and financial support as I worked to complete my thesis and degree.

TABLE OF CONTENTS

LIST OF TABLES

LIST OF FIGURES

CHAPTER 1

Introduction

1.1 Motivation

The goal of this thesis is to analyze, simulate and design a hybrid coupler phase shifter which will be utilized in a two-element phased antenna array. The phase shifter will provide a switched phase shift on one element of the array to change the beam direction of the array.

A phase shifter is a two-port microwave device which shifts the phase of an input signal. These devices are used in phased antenna arrays, radar arrays and other communications systems. A simplified phase shifter is shown in figure 1.1.

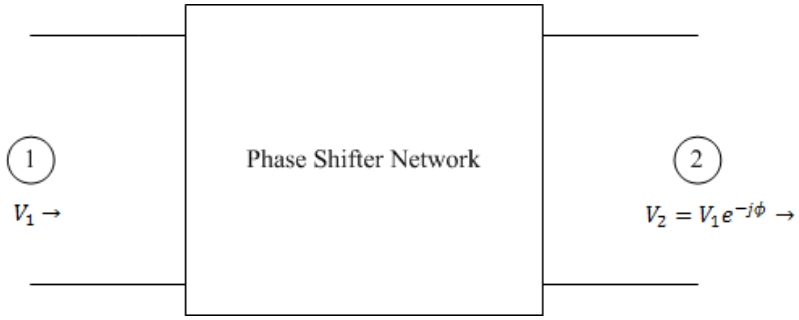

Figure 1.1: Simplified Phase Shifter

There are several methods of realizing a phase shifter. Early phase shifter

designs were simply mechanically adjusted transmission lines which would change the length of delay by adjusting the length of the transmission line [3]. Electronically adjustable shifters followed with ferrite based shifters. These shifters are all based on the interaction between an applied electromagnetic field and a ferrite and are typically used in waveguide applications [4]. The last major category of electronically adjustable shifters are semiconductor shifters which use p-i-n diodes, varactors or various FETs as switching elements. These shifters typically have switched elements or transmission line which provide a different phase shift on the output. FET phase shifters can also be used in active phase shifters which provide gain and a phase shift [5; 6]. Bulk and surface acoustic wave (BAW and SAW) implementations have also been developed [3].

One implementation of an electronically adjustable phase shifter uses a hybrid coupler at its center with several other components added onto its output ports to provide reflections which cancel on the input port and sum to a phase shifted version of the input on the fourth port. It is easily constructed using available resources, requires a low amount of external components, and is one of the most common forms used in practice [1]. An example of this implementation is shown in figure 1.2.

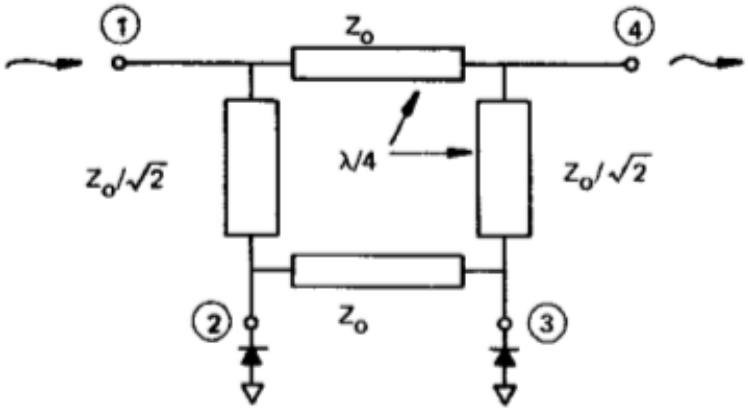

Figure 1.2: Hybrid Coupler Phase Shifter [1]

1.2 Problem Statement

1.2.1 Hybrid Coupler

The hybrid coupler is a four-port microwave device which takes an input on one port and provides an even power split on two output ports with a 90 degree phase shift between them. The fourth port on the device is isolated from the first. The device exhibits reciprocal behavior because any port can act as an input, and the device will operate in the same manner (albeit with different output ports) [2].

The coupler is made of four sections of quarter wavelength transmission line. Two sections have a characteristic impedance of Z_0, and the other two have an impedance of $Z_0/\sqrt{2}$. Each port is fed with a transmission line of impedance Z_0 [2].

A coupler can be categorized by five main parameters: bandwidth, insertion loss, coupling ratio, phase shift between ports, and isolation. Bandwidth is defined as the frequency range where the device provides a phase shift within ±10 degrees of the desired phase shift. Insertion loss is the additional loss within the device above the loss due to splitting. This can be caused by reflections of signals, dielectric losses, and conductor losses. Coupling ratio is defined as the ratio of the lower of the two output powers to the input power. Isolation refers to the ratio between the input power and the leakage power at the isolated port [7].

It will be necessary to have an idea of the typical specifications that commercially available hybrid couplers possess in order to gauge the performance of the constructed coupler. Hybrid couplers tend to have bandwidths of about 13:1 at a maximum. Over this bandwidth, couplers will typically exhibit about 3 dB of insertion loss, a coupling ratio of 3 dB and isolation of 20 dB [7].

1.2.2 Hybrid Coupler As a Phase Shifter

When the hybrid coupler is implemented as a phase shifter, the output ports are terminated with reactive (capacitive or inductive) loads. These reactances cause a reflection, which, when combined, will cause an output on the fourth port that is phase shifted by a certain degree from the input. The reactances are also typically either switched or analog variable to allow for a switched phase difference to be

obtained from the device [3]. The implementation used for this design will be two switched reactances.

Phase shifters are categorized by several parameters: phase response over bandwidth, insertion loss, and its desired switched phase shift [3]. Specifications of typical phase shifters tend to have about 2-3 dB of insertion loss, 90 or 180 degrees of switched phase shift (i.e. switching between 0 and 90/180 degrees of shift), and a 10% bandwidth. This bandwidth is the frequency range over which the device exhibits a phase shift that is ± 10 degrees from the desired phase shift [3; 1].

1.3 Summary of Prior Work

The basic design of a hybrid coupler phase shifter has been reported in both [1] and [8]. These papers provide a general guideline for designs, but do not give much information on the performance of these devices. This thesis will provide additional analysis of the device alongside simulation and experimental data to give expected results for future designs.

1.4 Organization of Thesis

Chapter 2 provides an analysis of the hybrid coupler phase shifter. It begins with an analysis of the hybrid coupler device which is followed by an analysis of the coupler implemented as a phase shifter.

Chapter 3 will focus on the simulation, design, construction and testing of the hybrid coupler. There will also be a discussion of the results for each iteration of the device.

Chapter 4 will present a discussion on the simulation, design, construction and testing of the hybrid coupler phase shifter. As in Chapter 3, there will be a discussion of the measurement results.

Chapter 5 will give a final discussion on the overall results of the work performed. There will also be a section to outline simulation and design lessons learned as well as suggestions for future work.

CHAPTER 2

Hybrid Coupler as Phase Shifter

This chapter will provide an analysis of both the hybrid coupler and phase shifter implementation as a basis for designing the hybrid coupler phase shifter.

2.1 S-Parameters

The hybrid coupler will be characterized by its S matrix which can be found using S-parameter analysis. This matrix will give the coupler's performance at the center frequency, but can also be found across a frequency band to understand the coupler's performance over a bandwidth. This information will then be used as the basis for deriving the S matrix of the phase shifter implementation to determine the shifter's behavior.

S-parameters relate incident and reflected voltage waves at the different ports of a microwave network. This relationship is defined to be

$$[V^-] = [S][V^+] \tag{2.1}$$

where V^- is the reflected voltage wave vector, V^+ is the incident voltage wave

vector, and S is the S matrix. The elements of these matrices are all complex numbers to account for both magnitude and phase.

The elements of the S matrix are defined as

$$[S_{ij}] = \frac{V_i^-}{V_j^+}\bigg|_{V_k^+=0, k\neq j} \tag{2.2}$$

where i is the port of the reflected wave and j is the port of the incident wave.

2.2 Analysis of Hybrid Coupler

The basic layout for a microstrip hybrid coupler is shown in figure 2.1. The hybrid coupler can be analyzed using an even-odd mode technique. This technique can be used because the coupler is a linear device. Linearity allows for the use of superposition to split an input source into a sum of even (in phase) and odd (out of phase) sources. This split allows the symmetry of the coupler to be preserved which simplifies analysis. Once the source is split, each mode can be analyzed separately and the sum of the results gives the total response of the coupler [9].

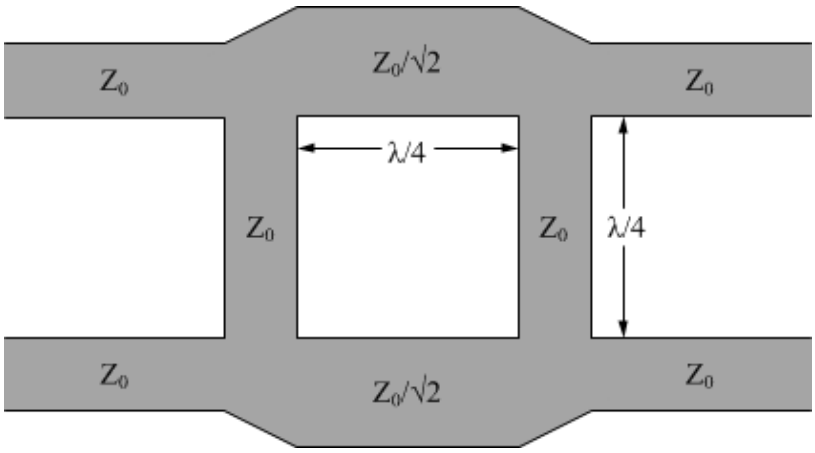

Figure 2.1: Hybrid Coupler Geometry

The first step in this analysis is to redraw the coupler as a normalized (with normalization constant Z_0, the characteristic impedance of the output ports) circuit schematic as shown in figure 2.2.

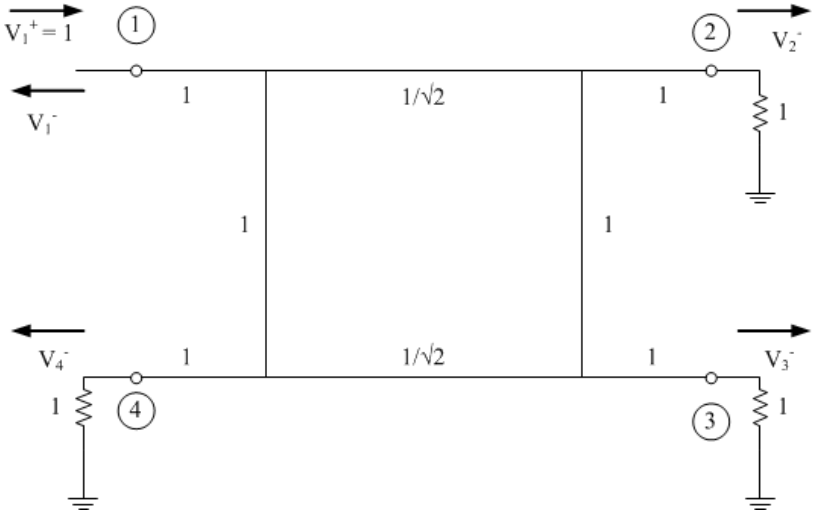

Figure 2.2: Hybrid Coupler Normalized Circuit Schematic

To find the S parameters of the coupler, the circuit needs to be excited at one

port while all other ports are terminated with a matched load. Once the reflected waves are found, the S parameters of the coupler can be determined by (2.2).

Port 1 is chosen arbitrarily as the first input port. As seen in figure 2.2, V_1^+ is incident on port 1, and we have reflected waves at each port ($V_1^-, V_2^-, V_3^-,$ and V_4^-). This excitation can be split into its even and odd modes as shown in figure 2.3.

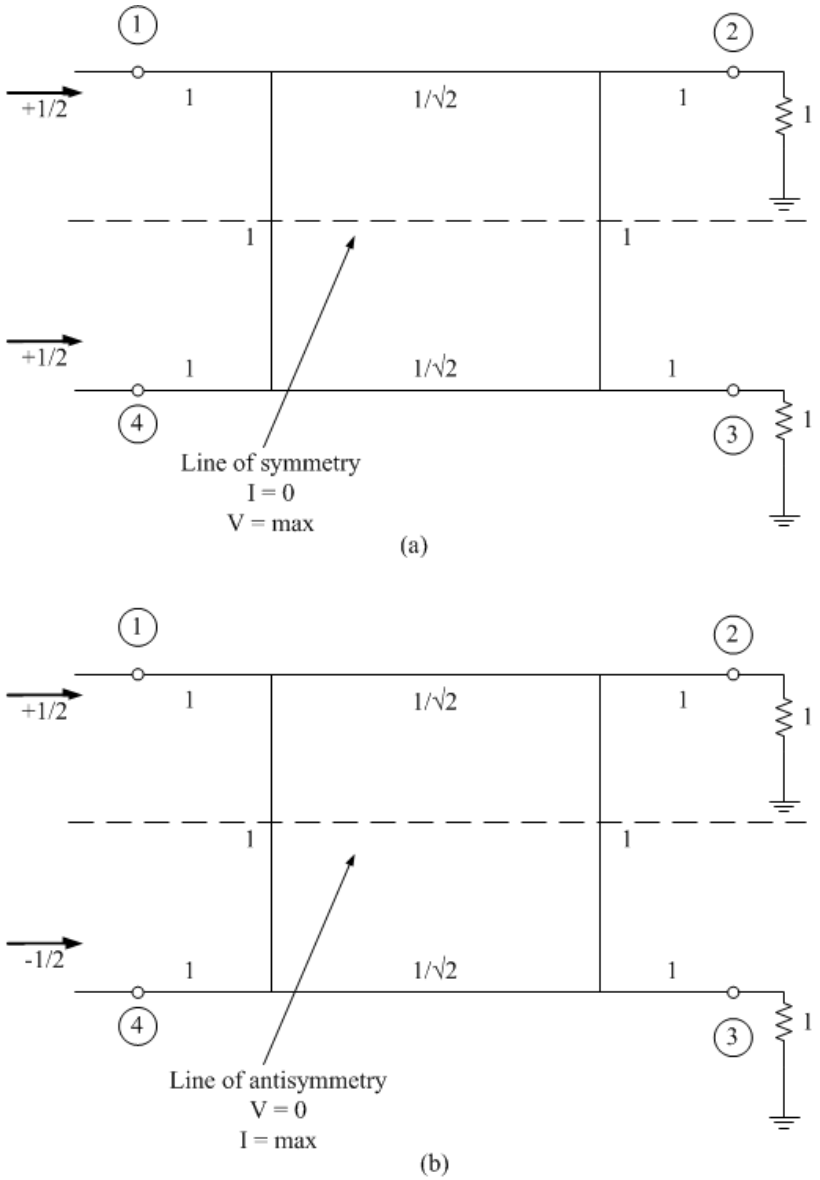

Figure 2.3: Hybrid Coupler Decomposition Into Even (a) and Odd (b) Modes

For the even mode analysis in figure 2.3a, the voltage sources are equivalent. The equivalent sources imply that there is no current at the line of symmetry. Having no current at this point allows the vertical traces to be represented as open circuited stubs with length $\lambda/8$. Now, there are two two-port networks (a network with ports 1, 2 and another with ports 3, 4); these two networks are identical which means only one of them needs to be analyzed. The easiest way to find the S parameters of one of the two-port networks is to use transmission (or ABCD) matrices to cascade the stubs and quarter-wavelength section. Additional information on transmission matrices and the conversion to S parameters can be found in Appendix A. The transmission matrix between ports 1 and 2 is

$$\begin{bmatrix} A & B \\ C & D \end{bmatrix}_e = [T_1][T_2][T_1] = \frac{1}{\sqrt{2}} \begin{bmatrix} -1 & j \\ j & -1 \end{bmatrix} \tag{2.3}$$

where subscript e represents a parameter associated with the even mode analysis, T_1 is the transmission matrix for the open circuit $\lambda/8$ length stub and T_2 is the transmission matrix of the quarter wavelength section.

T_1 is defined to be

$$\begin{bmatrix} 1 & 0 \\ j & 1 \end{bmatrix} \tag{2.4}$$

T_2 is defined to be

$$\begin{bmatrix} 0 & j/\sqrt{2} \\ j/\sqrt{2} & 0 \end{bmatrix} \tag{2.5}$$

Converting (2.3) to S parameters gives the reflection (Γ_e) and transmission (T_e) coefficients for the even mode as

$$\Gamma_e = \frac{A + B - C - D}{A + B + C + D} = 0 \tag{2.6a}$$

$$T_e = \frac{2}{A + B + C + D} = \frac{-1}{\sqrt{2}} - \frac{j}{\sqrt{2}} \tag{2.6b}$$

$A, B, C,$ and D are the elements of the transmission matrix from (2.3).

For the odd mode analysis in figure 2.3b, the two voltage sources are equal in magnitude but out of phase. This odd symmetry of the sources leads to zero voltage at the line of antisymmetry. The vertical transmission lines in this case are short circuit stubs with length $\lambda/8$. Using the same approach as the even mode, the S parameters can be found by using the transmission matrices as

$$\begin{bmatrix} A & B \\ C & D \end{bmatrix}_o = [T_3][T_2][T_3] = \frac{1}{\sqrt{2}} \begin{bmatrix} 1 & j \\ j & 1 \end{bmatrix} \tag{2.7}$$

where subscript o represents a parameter associated with the odd mode analysis and T_3 is the transmission matrix for the short circuit $\lambda/8$ length stub.

T_3 is defined to be

$$\begin{bmatrix} 1 & 0 \\ -j & 1 \end{bmatrix} \tag{2.8}$$

Converting this result to S parameters gives the reflection (Γ_o) and transmission (T_o) coefficients for the odd mode as

$$\Gamma_o = \frac{A + B - C - D}{A + B + C + D} = 0 \tag{2.9a}$$

$$T_o = \frac{2}{A + B + C + D} = \frac{1}{\sqrt{2}} - \frac{j}{\sqrt{2}} \tag{2.9b}$$

where $A, B, C,$ and D are the elements of the transmission matrix from (2.7).

Based on the polarity of the odd and even mode excitations, the total response of the system can be found to be

$$S_{11} = \frac{1}{2}\Gamma_e + \frac{1}{2}\Gamma_o = 0 \tag{2.10a}$$

$$S_{21} = \frac{1}{2}T_e + \frac{1}{2}T_o = \frac{-j}{\sqrt{2}} \tag{2.10b}$$

$$S_{31} = \frac{1}{2}T_e - \frac{1}{2}T_o = \frac{-1}{\sqrt{2}} \tag{2.10c}$$

$$S_{41} = \frac{1}{2}\Gamma_e - \frac{1}{2}\Gamma_o = 0 \tag{2.10d}$$

Eqns. 2.10 show that, at the center frequency, this design will have no reflection at the input port (from (2.10a)), no output at the isolation port (from (2.10d)), and outputs that are shifted 90 and 180 degrees from the input at the output ports (from

(2.10b) and (2.10c), respectively). The output ports are also shifted 90 degrees in phase from each other. These are the desired results from a hybrid coupler.

Based on the symmetry of the circuit, the rest of the S parameters can be deduced. The final S matrix for the hybrid coupler is

$$[S] = \frac{1}{\sqrt{2}} \begin{bmatrix} 0 & -j & -1 & 0 \\ -j & 0 & 0 & -1 \\ -1 & 0 & 0 & -j \\ 0 & -1 & -j & 0 \end{bmatrix} \tag{2.11}$$

This S matrix is very idealized. Practically, there will always be some reflection at the input port and some power delivered to the isolated port. Also, there is loss in the transmission line sections. Together, these losses will cause the power delivered to the output ports to be less than the -3 dB that is expected in the ideal case.

2.3 Analysis of Phase Shifter Implementation

Using the analysis results of the hybrid coupler, the behavior of the hybrid coupler phase shifter can be found. Using (2.2), it is possible to find the reflected voltages at ports one and four of the device when excited at port one with loads terminated on ports two and three [1].

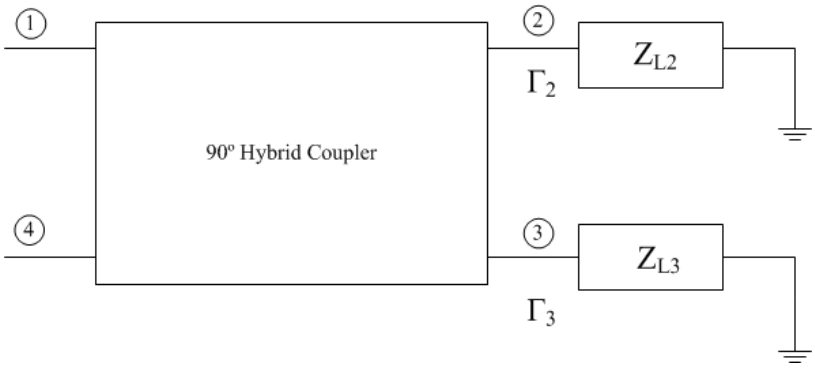

Figure 2.4: Hybrid Coupler Phase Shifter

Z_{L2} and Z_{L3} are the load impedances and Γ_2 and Γ_3 are the reflection coefficients due to the load at ports 2 and 3, respectively. With loads placed on ports 2 and 3, this circuit takes an input at port 1 or 4 and provides a phase shifted version of the signal on port 4 or 1 due to the reciprocal nature of the coupler. For the following analysis, port 1 is arbitrarily chosen as the input and port 4 is chosen as the output. From figure 2.4, the incident voltage waves can be defined as

$$V_1^+ = V_0 \tag{2.12a}$$

$$V_2^+ = \Gamma_2 V_2^- \tag{2.12b}$$

$$V_3^+ = \Gamma_3 V_3^- \tag{2.12c}$$

$$V_4^+ = 0 \tag{2.12d}$$

where Γ_2 and Γ_3 are the reflection coefficients at ports two and three, respectively, and V_0 is the incident voltage amplitude. Eqn. 2.12a is the voltage wave at the

driven port in the analysis, and therefore is arbitrarily chosen as V_0. The incident waves in (2.12b) and (2.12c) are due to the reflection of the output waves from ports 2 and 3, respectively. The incident voltage on port 4 is 0 because the port is terminated in a matched load in order to satisfy the conditions of (2.2).

Using (2.2), (2.11), and (2.12), the reflected voltage waves can be found to be

$$V_1^- = \frac{-j}{\sqrt{2}} V_2^+ + \frac{-1}{\sqrt{2}} V_3^+ \tag{2.13a}$$

$$V_2^- = \frac{-j}{\sqrt{2}} \Gamma_2 V_1^+ \tag{2.13b}$$

$$V_3^- = \frac{-1}{\sqrt{2}} \Gamma_3 V_1^+ \tag{2.13c}$$

$$V_4^- = \frac{-1}{\sqrt{2}} V_2^+ + \frac{-j}{\sqrt{2}} V_3^+ \tag{2.13d}$$

Substituting these equations into (2.13a) shows that in order to have no reflected voltage at port one, Γ_2 and Γ_3 must be equal (replaced now by Γ). By substituting for Γ and the reflected waves, the output at port 4 can be found to be

$$V_4^- = j\Gamma V_1^+ \tag{2.14}$$

which is a phase shifted version of the input because

$$\Gamma = |\Gamma| e^{-j\phi} \tag{2.15}$$

where ϕ is the phase angle of the reflection coefficient. In order to not introduce any additional loss into the phase shifter, $|\Gamma|$ must be equal to 1. For practical applications, it is impossible to achieve perfect reflection from a load which means that some power will be dissipated in the load and $|\Gamma|$ will be less than one. Therefore, some loss will always occur between the input and output signals. This analysis also assumes an ideal hybrid coupler which is impractical to build. A realistic coupler will not have a perfect 3 dB power split or provide a 90 degree phase shift across the entire band; this will cause additional attenuation of the phase shifted signal as well as introduce more reflection at the input port due to imperfect cancellation of the reflected signals. However, these degradations will not significantly degrade the performance of the phase shifter.

CHAPTER 3

Hybrid Coupler Design

In order to construct a hybrid coupler phase shifter, the hybrid coupler at its center must be built first. This chapter will cover the design goals and design process for the hybrid coupler.

3.1 Design Goals

The goal for this hybrid coupler design will be to have approximately 10% bandwidth over which it exhibits greater than 1 dB of return loss, a coupling ratio of 3 dB (±0.5 dB) and isolation of 15 dB with a center frequency of 1800 MHz.

3.2 First Iteration

The hybrid coupler for this design will be matched to ports with 50 ohm impedance. Because of this, the quarter-wavelength sections of the device have 50 and 35.4 ohm impedances. The coupler will be built out of microstrip on a substrate of RT Duroid 5870. The characteristics of this board are presented in table 3.1 [10].

Parameter	Value
Dielectric constant, ϵ_r	2.33
Loss tangent, δ	0.0008
Ground plane thickness	1.38 mils
Trace thickness	1.25 mils
Substrate thickness	62 mils

Table 3.1: RT Duroid 5870 Characteristics

3.2.1 Design

For the first design, the widths of the traces were calculated using the formulation in [2]. The design parameters are shown in table 3.2.

Parameter	Dimension
50 Ω trace width	182.4 mils
35.4 Ω trace width	299.4 mils
Quarter-wavelength ($\epsilon_r = 2.33$)	1.0747 inches

Table 3.2: Design 1 Trace Dimensions

The final layout is shown in figure 3.1.

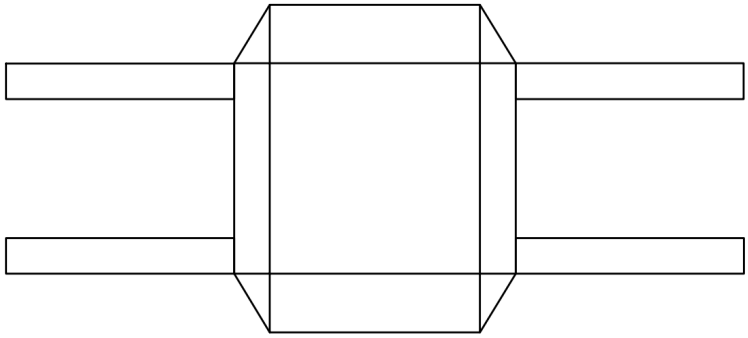

Figure 3.1: Design 1 Trace Layout

3.2.2 Simulation

An initial simulation of this circuit was created in RF Sim to verify design widths and lengths. The phase velocity through the microstrip lines can be found using

$$v_{ph} = \frac{1}{\sqrt{\mu\epsilon}} = 1.96 * 10^8 \ {}^{m}/_{s} \tag{3.1}$$

The phase velocity of the microstrip can then be set in RF Sim along with the quarter-wavelength section lengths to get the simulation circuit in figure 3.2.

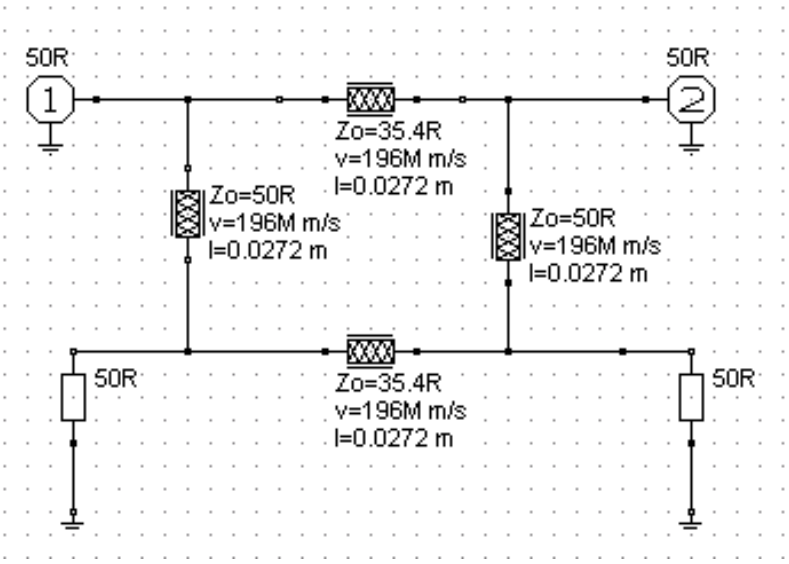

Figure 3.2: Simulation for Hybrid Coupler Design 1

Figure 3.3 shows the reflection coefficient at each port of the coupler in dB over the frequency range of 1-3 GHz. This plot shows a deep null at 1800 MHz which indicates a very good match at that frequency to 50 Ω. This is very desirable because there will be maximum power delivered to the device at this frequency.

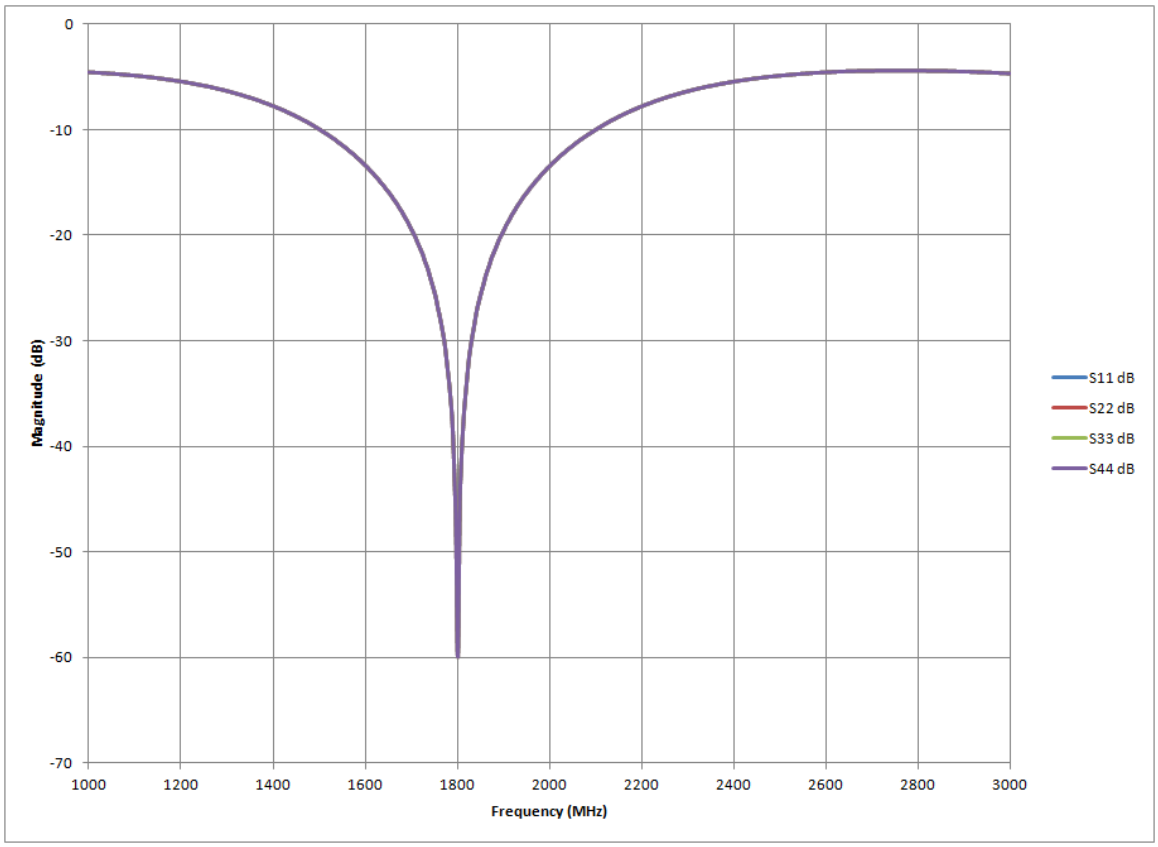

Figure 3.3: Simulation 1 Reflection Coefficients

Figure 3.4 shows the transmission coefficients from port 1 to ports 2 and 3 (in dB) across the same frequency band as the reflection coefficients. At 1800 MHz, the desired -3 dB value is reached with a wide bandwidth where the two coefficients are within 0.5 dB of -3 dB. This will provide an even power split at the design frequency and close to even across the band.

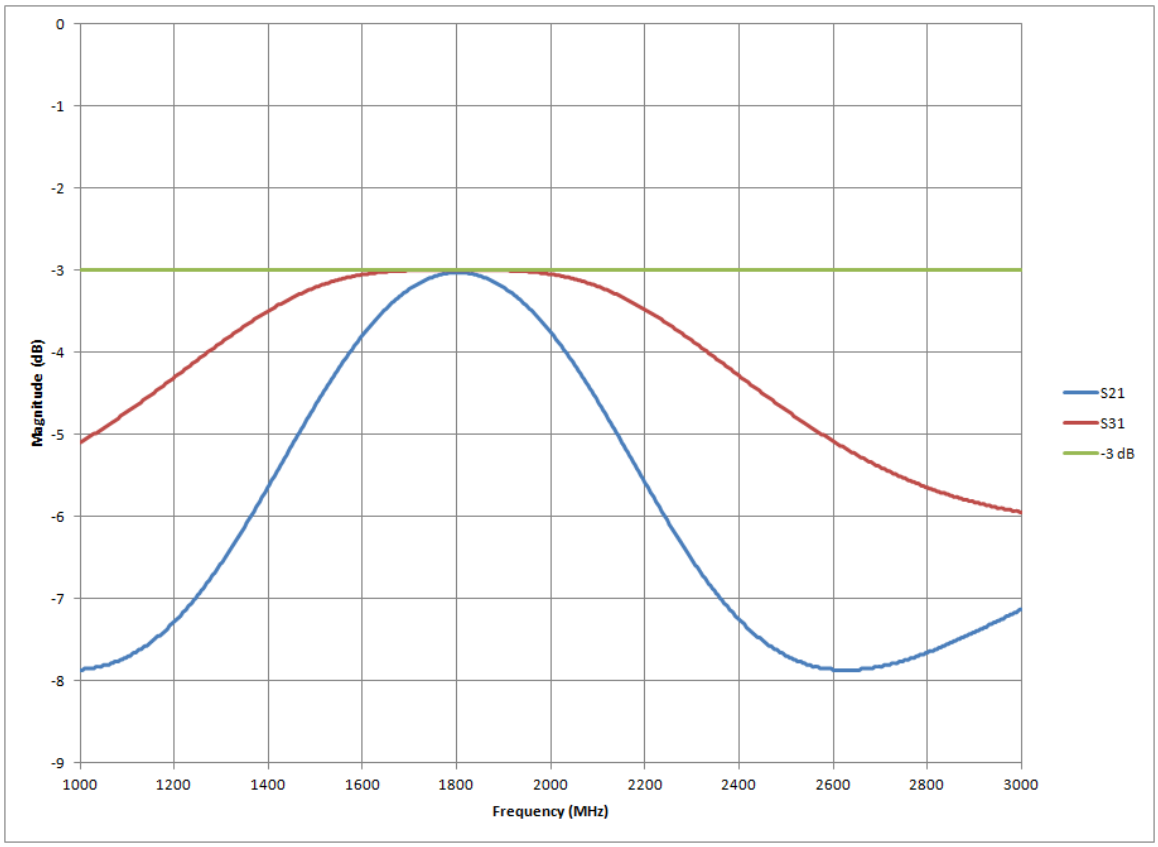

Figure 3.4: Simulation 1 Transmission Coefficients

Figure 3.5 shows the isolation level in dB from port 1 to port 4 over the frequency range of 1-3 GHz. There is a deep null at 1800 MHz which means that there will be negligible power at the isolated port near the center frequency. This means that maximum power will be delivered to the output ports.

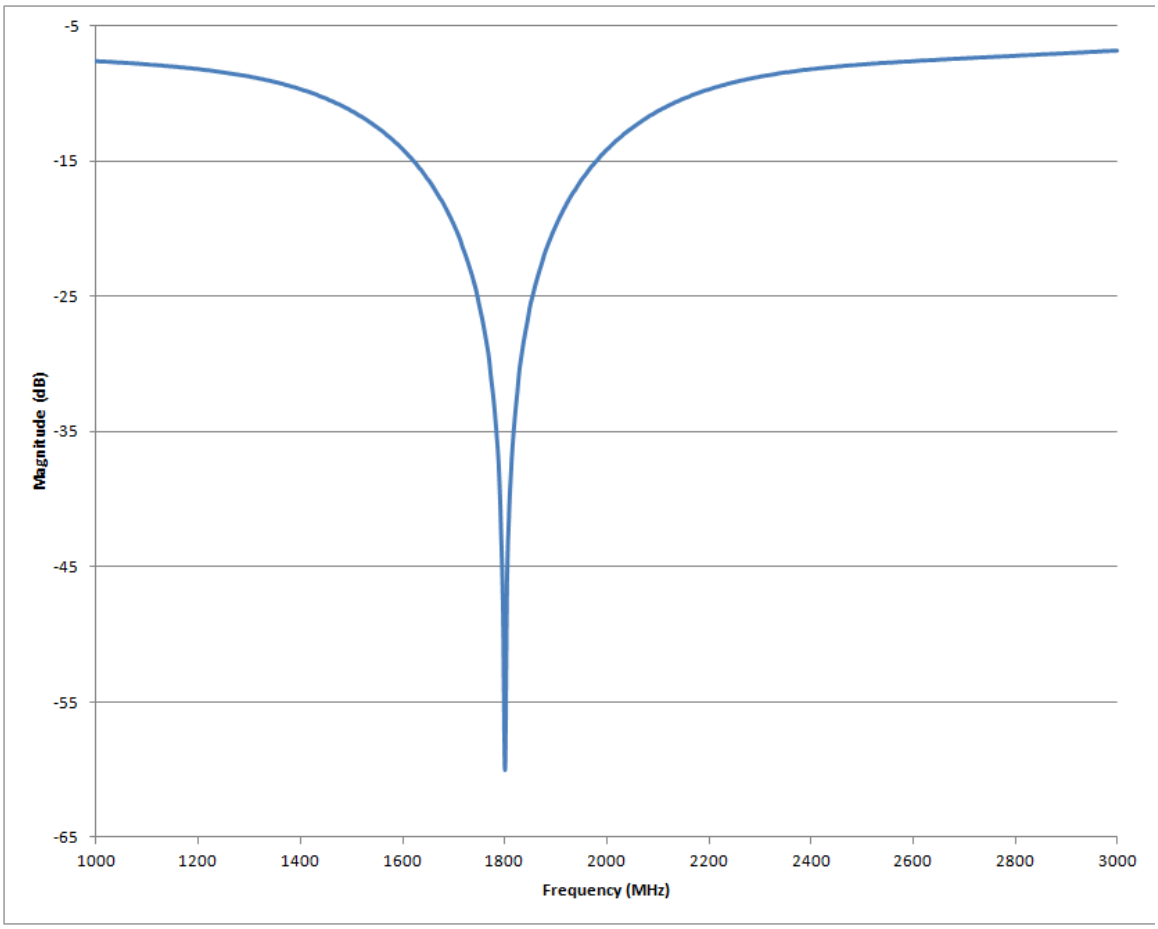

Figure 3.5: Simulation 1 Isolation

Figure 3.6 shows the difference in phase (in degrees) between ports 2 and 3. Recalling (2.11), the ideal phase difference between these two ports should be 90 degrees. There is a large bandwidth over which the coupler has a 90 degree phase shift between the two output ports.

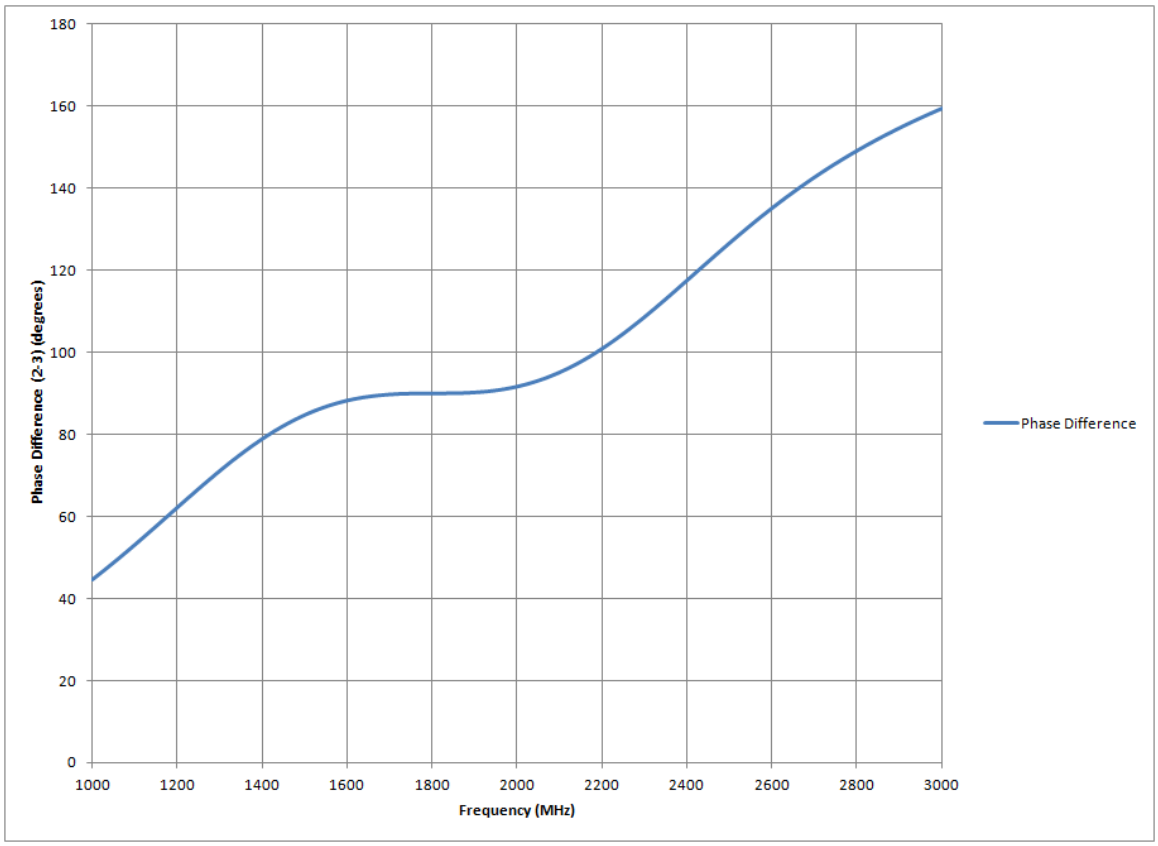

Figure 3.6: Simulation 1 Phase Difference

3.2.3 Construction

The first iteration of the coupler was constructed by hand. Copper tape (thickness 1.25 mils) was applied to the RT Duroid board. The layout of the design in figure 3.1 was placed on top of the tape and the traces were cut out using a utility knife. At each port, an SMA connector was soldered to the trace and to the ground plane for connecting the device to a network analyzer. The finished coupler is shown in figure 3.7.

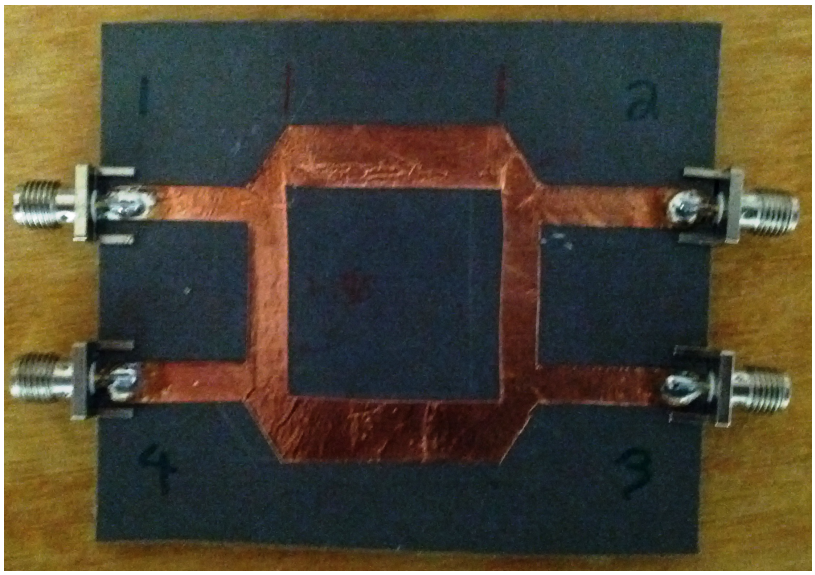

Figure 3.7: Design 1 Constructed Device

3.2.4 Testing

Once the coupler was constructed, measurements were performed to evaluate the performance of the coupler. These measurements were taken using an Agilent 8714ES Vector Network Analyzer.

Figure 3.8 shows the reflection coefficient at each port of the coupler in dB over the frequency range of 1-3 GHz. Ideally, these plots would all be identical and the deep null would be centered at 1800 MHz. The frequency of this null is the frequency were the port is best matched to 50 Ω (i.e. there is the least reflection). This plot shows that the device is not matched to 50 Ω at 1800 MHz, but rather somewhere between 1650-1700 MHz. The shallow nulls for S_{11} and S_{33} imply that

these two ports are much more poorly matched to 50 Ω across the frequency range than the other two ports.

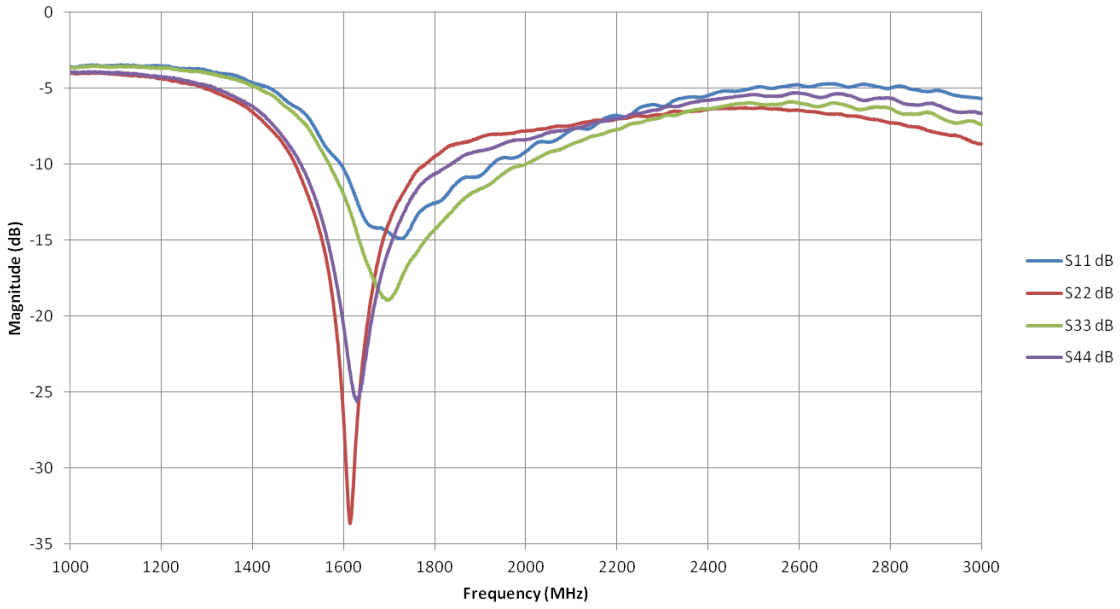

Figure 3.8: Design 1 Reflection Coefficients

Figure 3.9 shows the transmission coefficient magnitudes from port 1 to ports 2 and 3 (in dB) across the same frequency band as the reflection coefficients were measured. The expected value for these coefficients at 1800 MHz is -3 dB (indicated by the green line on the plot). When both coefficients are -3 dB, there is an even power split at the two output ports. The actual coefficients near 1650-1700 MHz (the center frequencies as determined from the reflection coefficients) are within ±1 dB of the desired value.

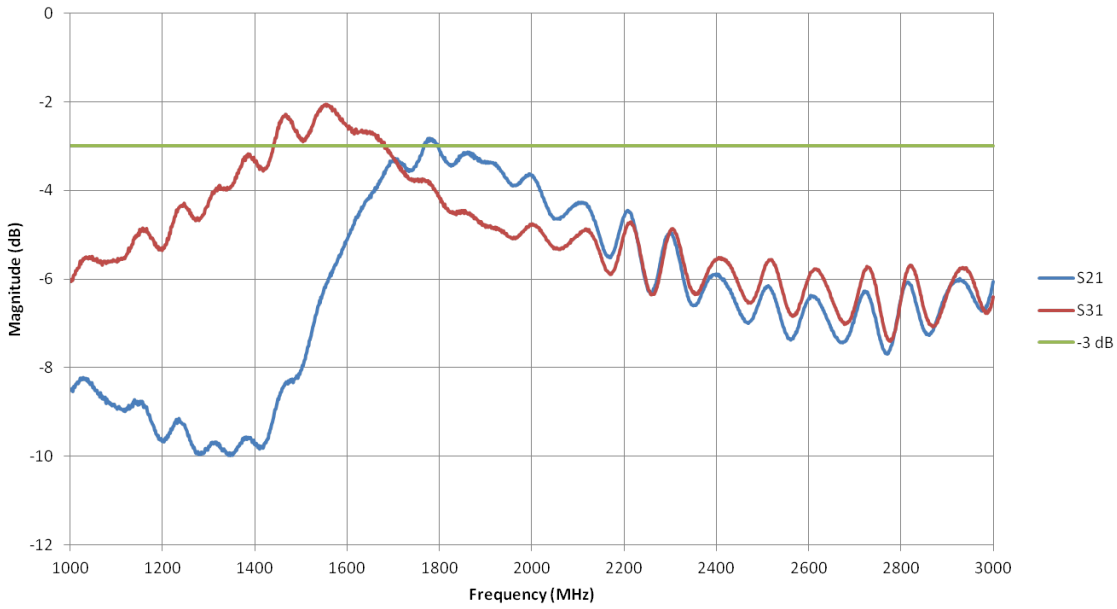

Figure 3.9: Design 1 Transmission Coefficients

Figure 3.10 shows the isolation level in dB from port 1 to port 4 over the frequency range of 1-3 GHz. The isolation coefficient null is located at the frequency where the minimum power from the input signal reaches port 4 (i.e. the port which is not used as the input or one of the outputs). When the isolation and reflection coefficient magnitudes are at minimums, there is maximum power available at the output ports; S_{21} and S_{31} are closest to -3 dB each. However, in this design, the center frequency is at 1650 MHz and not the desired 1800 MHz.

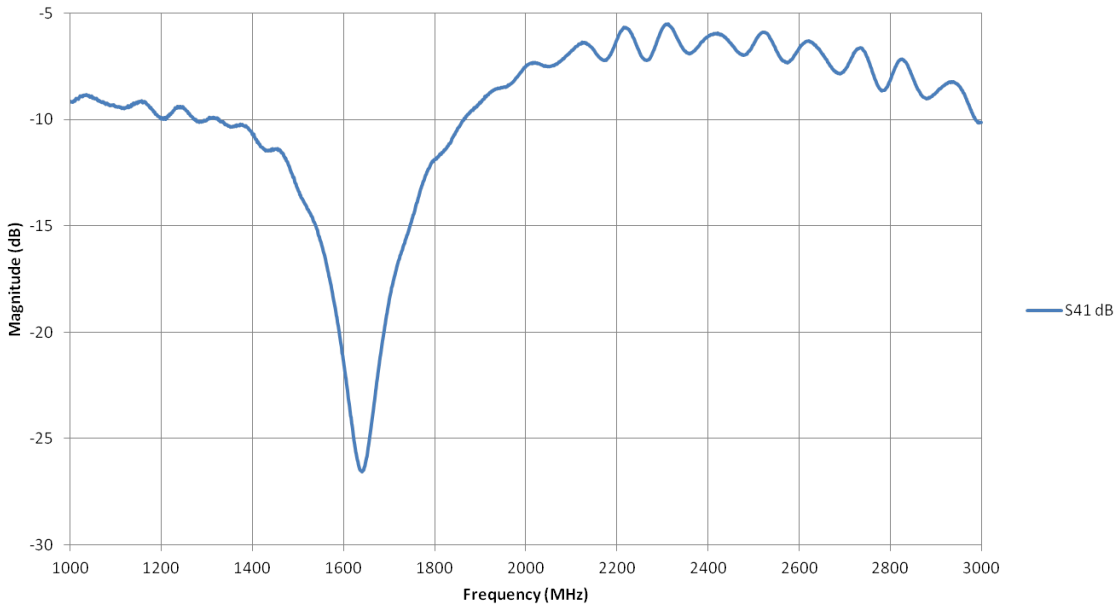

Figure 3.10: Design 1 Isolation

Figure 3.11 shows the difference in phase (in degrees) between ports 2 and 3. Recalling (2.11), the ideal phase difference between these two ports should be 90°. This plot shows that the phase difference does not reach 90° at any point between 1 and 3 GHz.

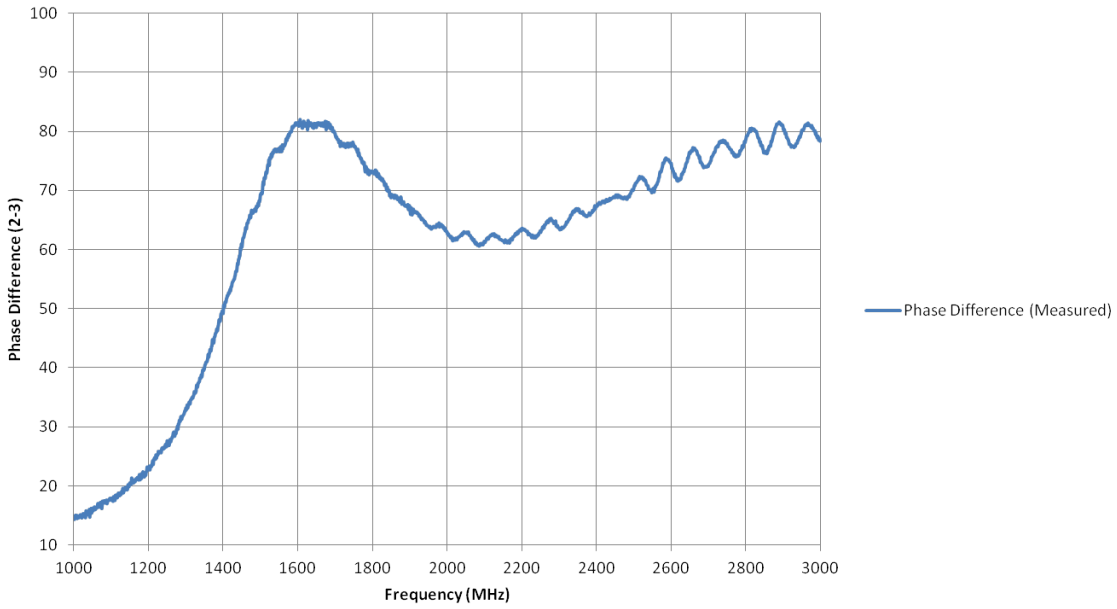

Figure 3.11: Design 1 Phase Difference

3.2.5 Discussion of Results

The first iteration results were not as expected. As noted in the previous section, the coupler's operating frequency was closer to 1650 MHz than to the design frequency of 1800 MHz. Although this design parameter was not met, the main discrepancy between simulation and measurement came in the phase shift between the output ports not being at or near 90 degrees in the band of operation. Further simulation and analysis of the design revealed several issues.

The first problem is that the design was developed using the relative dielectric constant, ϵ_r, and not the effective dielectric constant, ϵ_{eff}. ϵ_{eff} is a design

parameter for microstrip transmission line which is related to ϵ_r, the width of the trace, the frequency of operation, and the height of the substrate. It provides a way to account for some of the fields of the microstrip line being in the air, and some being in the substrate (see Appendix B for information on effective dielectric constants) [2]. Because of this, the lengths used for the quarter-wavelength sections were too long.

Another issue is that the t-junctions of the microstrip add additional capacitance and inductance to the circuit [11]. These junction parasitics can detract from the frequency performance of the coupler (see Appendix C for additional information on junction parasitics).

The final design issue is the placement of the quarter-wavelength sections (as seen in figure 3.12). This design used feeds as shown in 3.12a; the effective length of the 50 Ω branches was shorter than the design length due to this feed structure which caused the phase difference problems shown in figure 3.11. The feed trace layout in figure 3.12b maintains the correct length of the 50 Ω branches.

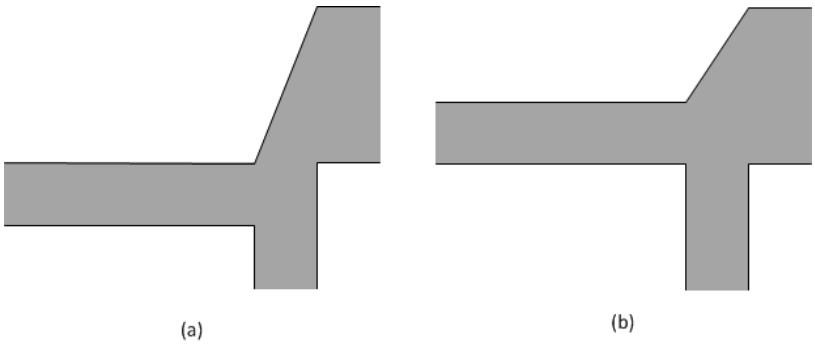

Figure 3.12: Feed Trace Layouts

In addition, there were most likely some errors caused by the hand construction of the device including, but not limited to, uneven trace widths and height variation of the copper due to creases in the copper tape from application to the substrate.

The RF SIM schematic was modified to account for many of these issues and is redrawn in figure 3.13.

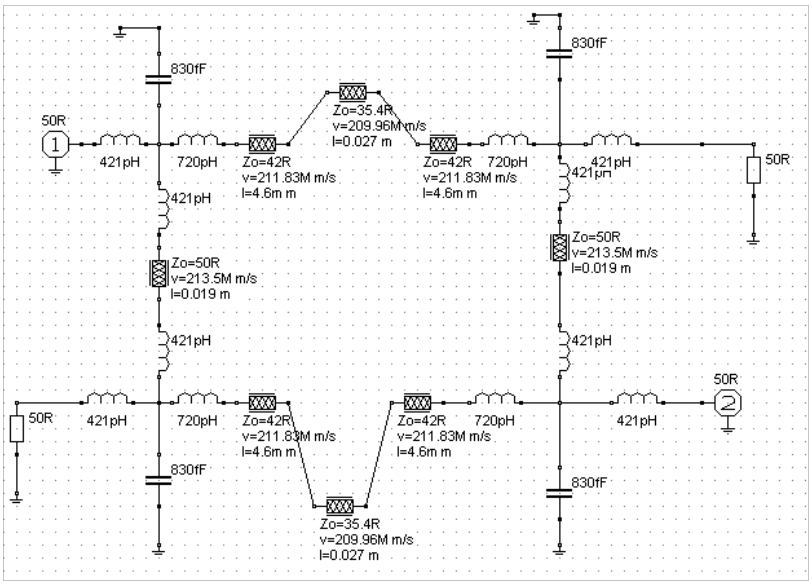

Figure 3.13: Updated Circuit for Simulation for Design 1

In the circuit of figure 3.13, the lengths of the 50 Ω traces were shortened, junction capacitance and inductance effects were added at all t-junctions (830 fF shunt capacitors, 421 pH inductors in series with the 50 Ω traces and 720 pH inductors in series with the 35.4 Ω traces.), additional traces (the short 42 Ω traces) were added between the feeds and the 35.4 Ω traces to account for the extra length due to the feed structure, and the phase velocities for all traces were updated to account for the effects of ϵ_{eff}. The values for the junction parasitics were calculated using equations found in Appendix C. Using this circuit, the simulation results more closely resembled the measured results from the device. The phase difference for the new simulation is shown in figure 3.14. The lines marking 80 and 100 degrees mark the desired range of operation for this design.

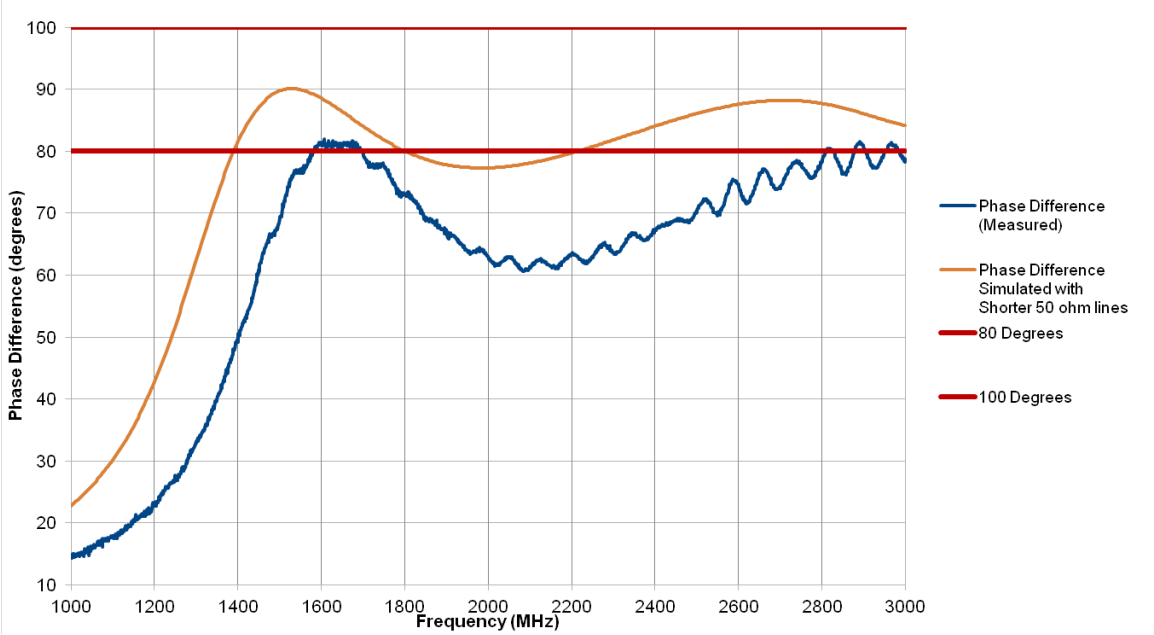

Figure 3.14: Design 1 Measured versus Simulated Phase Differences

The other measurements from the simulation closely matched the measured results.

3.3 Second Iteration

3.3.1 New Design

Fixing the errors in the first iteration allowed for the development of a new design. Correcting the design for the use of ϵ_{eff} gave new trace information as shown in table 3.3.

Parameter	Value
50 Ω ϵ_{eff}	1.9744
35.4 Ω ϵ_{eff}	2.0415
50 Ω trace width	183.8 mils
35.4 Ω trace width	300.8 mils
Quarter-wavelength (50 Ω)	1.167 inches
Quarter-wavelength (35.4 Ω)	1.148 inches

Table 3.3: Design 2 Trace Dimensions

The updated simulation circuit is shown in figure 3.15.

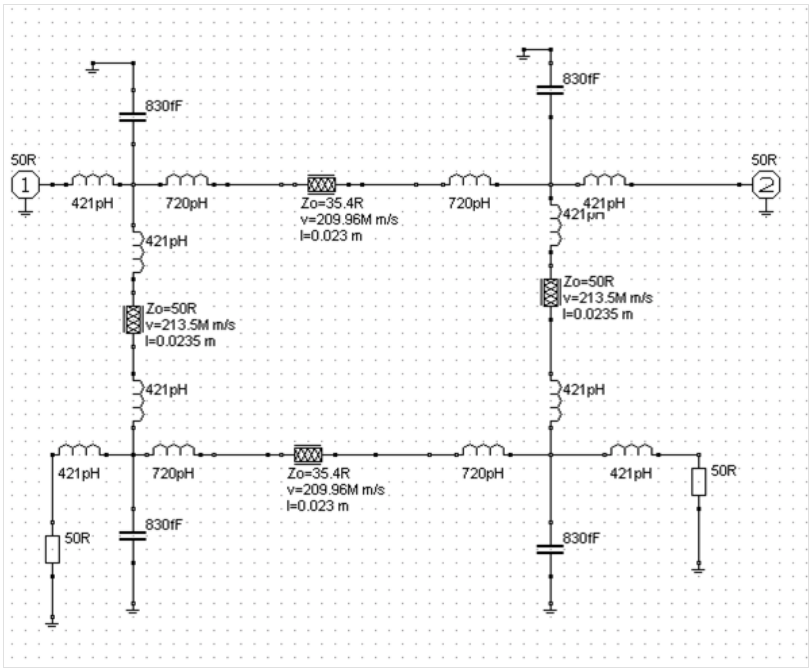

Figure 3.15: Simulation for Hybrid Coupler Design 2

Here, the line lengths and phase velocities have been updated to reflect the corrected values and junction effects have been included.

Figure 3.16 shows the reflection coefficients for the simulation circuit. Each port has a deep null at 1800 MHz which indicates a good match to 50 Ω at the center frequency.

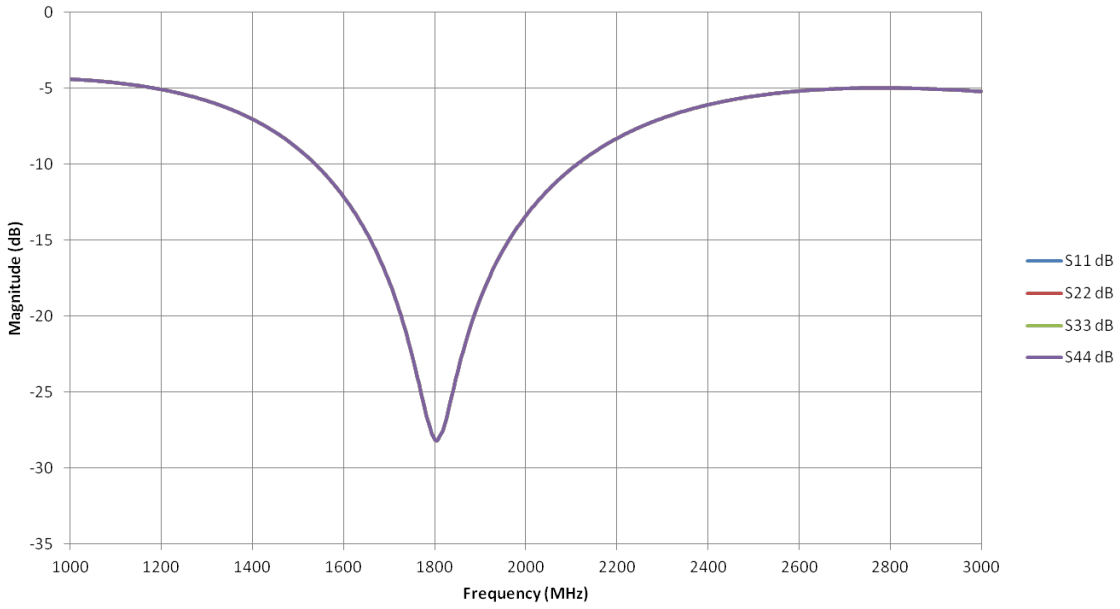

Figure 3.16: Simulation 2 Reflection Coefficients

Figure 3.17 is the updated transmission coefficients with port 1 as an input and ports 2 and 3 as outputs. These curves are within ±0.5 dB of -3 dB for both curves at the 1800 MHz which is the desired tolerance for the coupler.

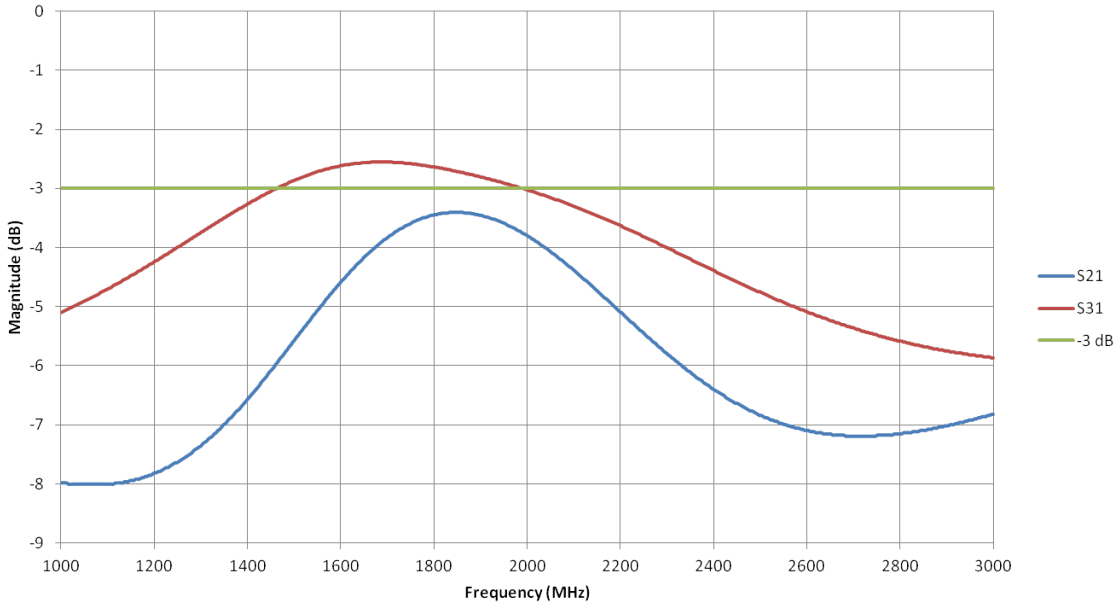

Figure 3.17: Simulation 2 Transmission

Figure 3.18 shows the isolation between ports 1 and 4. It has a deep null at 1800 MHz which means that port 4 is well isolated from port 1.

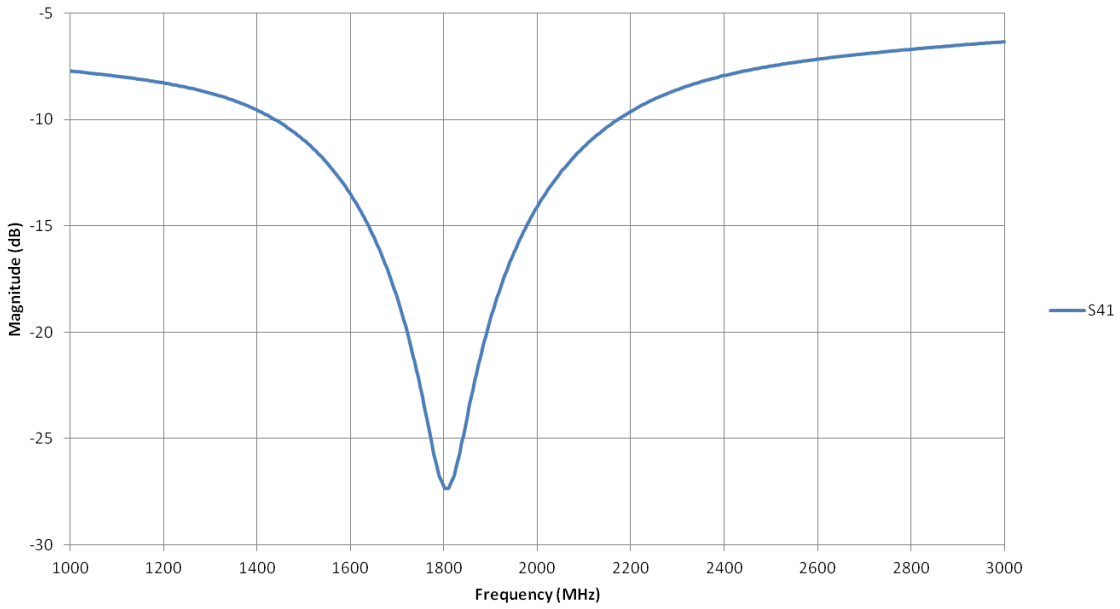

Figure 3.18: Simulation 2 Isolation

Figure 3.19 shows the phase difference between ports 2 and 3 with an input at port 1. The difference is 90 degrees at 1800 MHz and has a large bandwidth where the difference is between 80 and 100 degrees (to match design specifications).

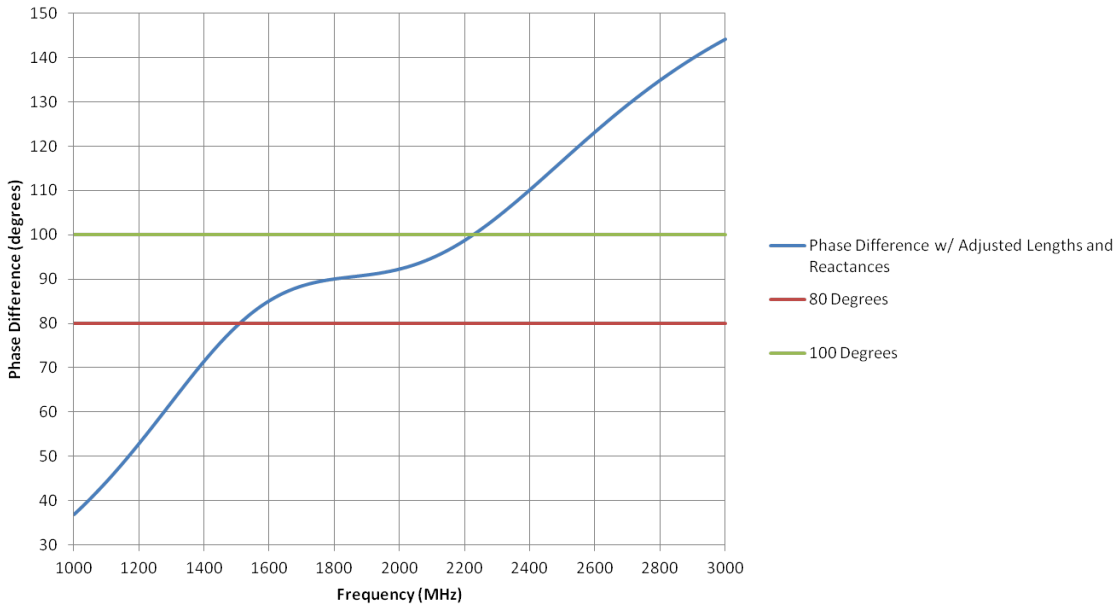

Figure 3.19: Simulation 2 Phase Difference

These updated simulation results demonstrate that, with parasitics and corrected trace lengths, a second iteration of a hybrid coupler can be constructed that will meet design specifications.

3.3.2 Construction

For the second design, the hybrid coupler was cut from double sided copper RT Duroid using a board router. This would give more consistent cuts along the traces than could be achieved by hand. Using the double sided board would also provide a smoother layer of copper than was seen with the hand laid tape. The board router used was a LKPF Protomat C40 Circuit Board Plotter. This machine

has a minimum resolution of 7.937 μm (0.312 mil) ($\pm$0.005mm (0.2 mil)) which is more than sufficient for the dimensions used in table 3.3 [12].

3.3.3 Testing

Testing the second design followed the same procedure that was used to measure the S parameters of the first iteration.

Figure 3.20 shows the reflection coefficient at each port of the coupler in dB over the frequency range of 1.5-3 GHz. Again, these plots should all be identical and the deep null would be centered at 1800 MHz. However, this device is matched more closely to 2050-2100 MHz.

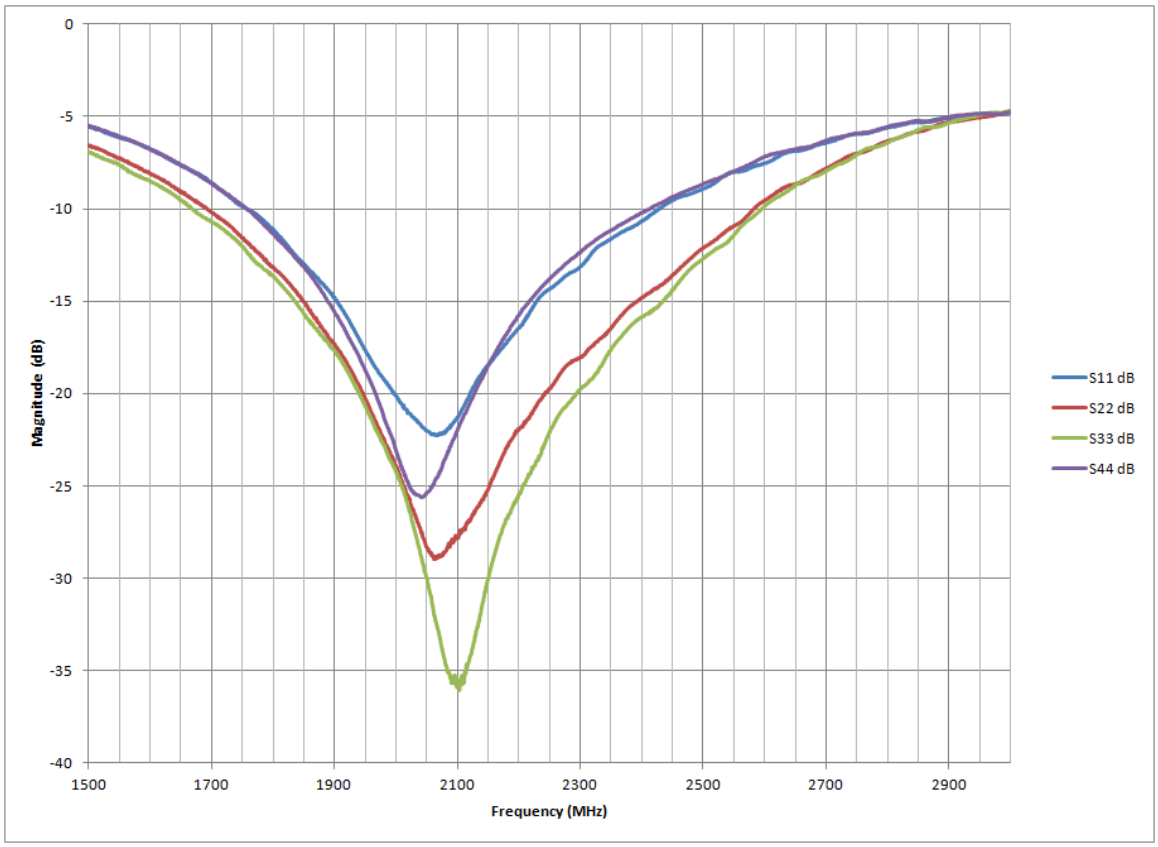

Figure 3.20: Design 2 Reflection Coefficients

Figure 3.21 shows the transmission coefficients from port 1 to ports 2 and 3 (in dB) across the same frequency band as the reflection coefficients were measured. The expected value for these coefficients at 1800 MHz is -3 dB (indicated by the green line on the plot). The actual coefficients near 2050-2100 MHz (the center frequencies as determined from the reflection coefficients) are within ±1 dB of the desired value.

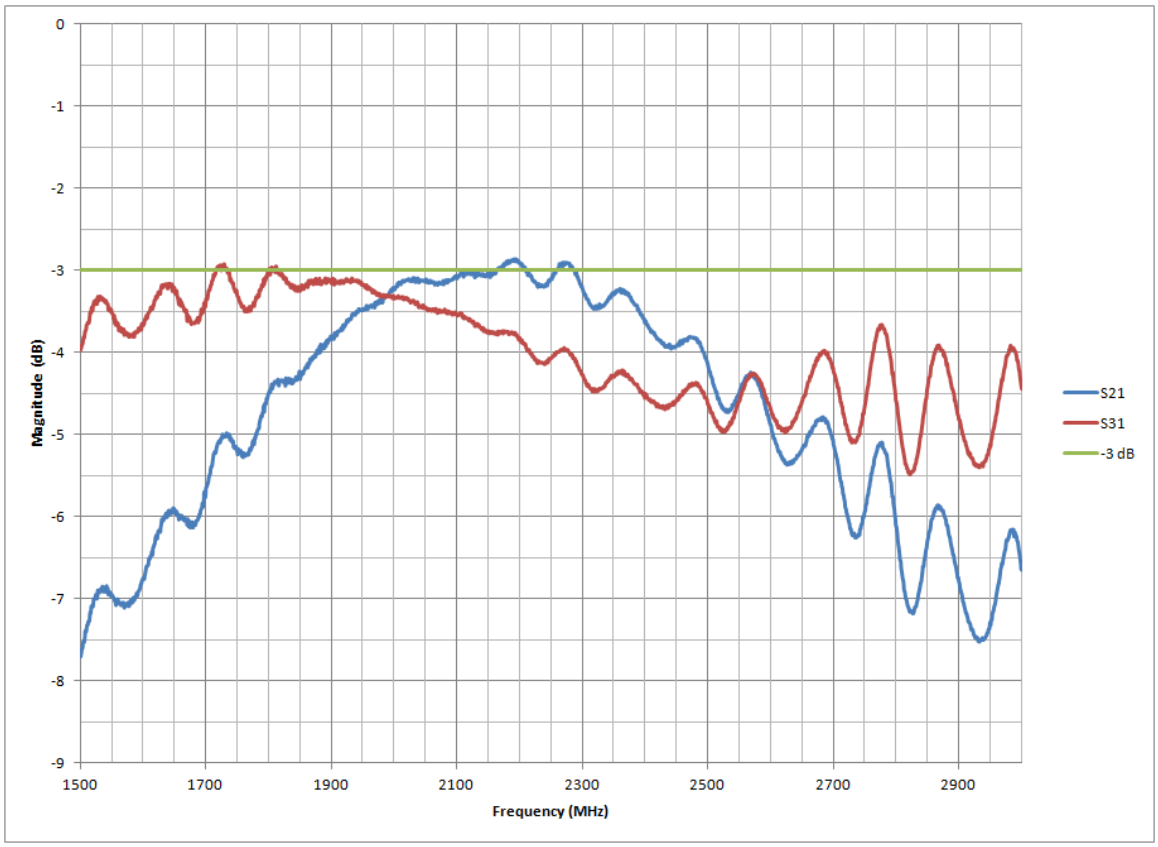

Figure 3.21: Design 2 Transmission Coefficients

Figure 3.22 shows the isolation level in dB from port 1 to port 4 over the frequency range of 1.5-3 GHz. However, in this design, the center frequency is at 2100 MHz and not the desired 1800 MHz.

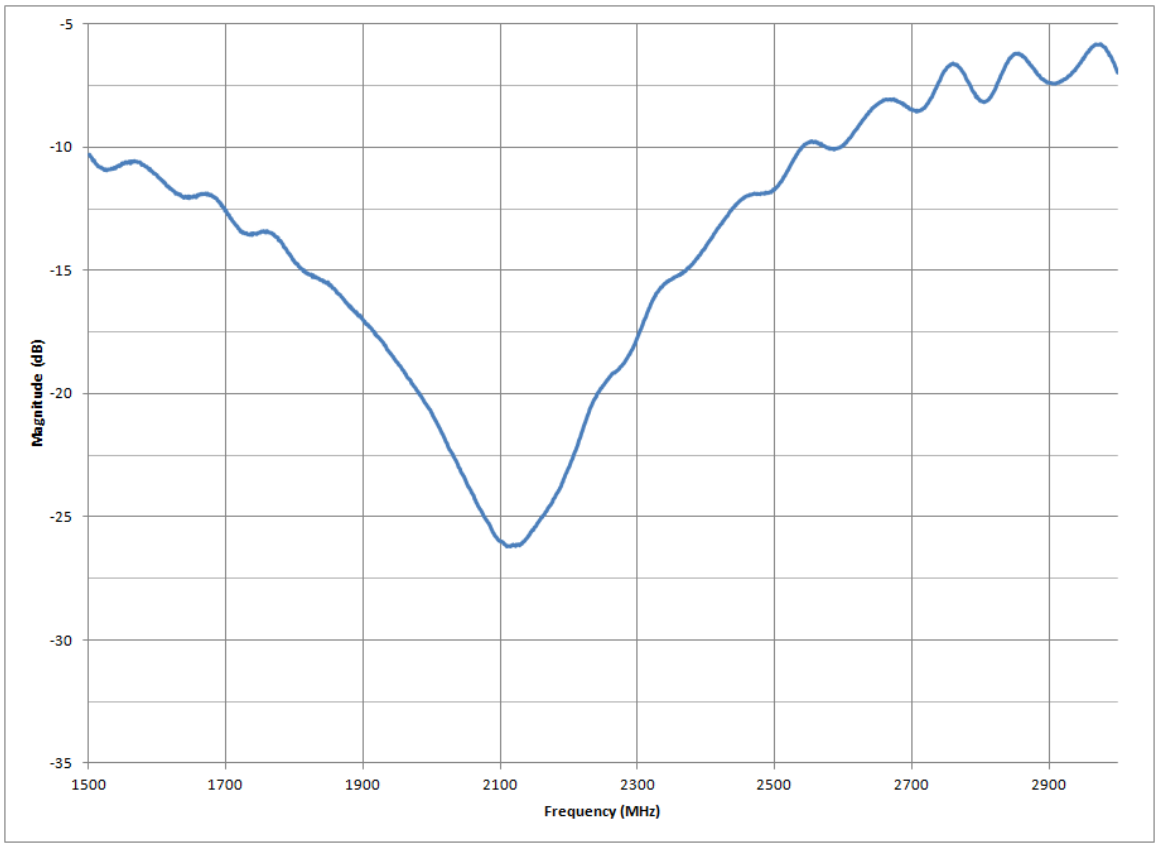

Figure 3.22: Design 2 Isolation

Figure 3.23 shows the difference in phase (in degrees) between ports 2 and 3. Recalling (2.11), the ideal phase difference between these two ports should be 90 degrees. This plot shows that the phase difference is within ± 3 degrees from 1850-2650 MHz.

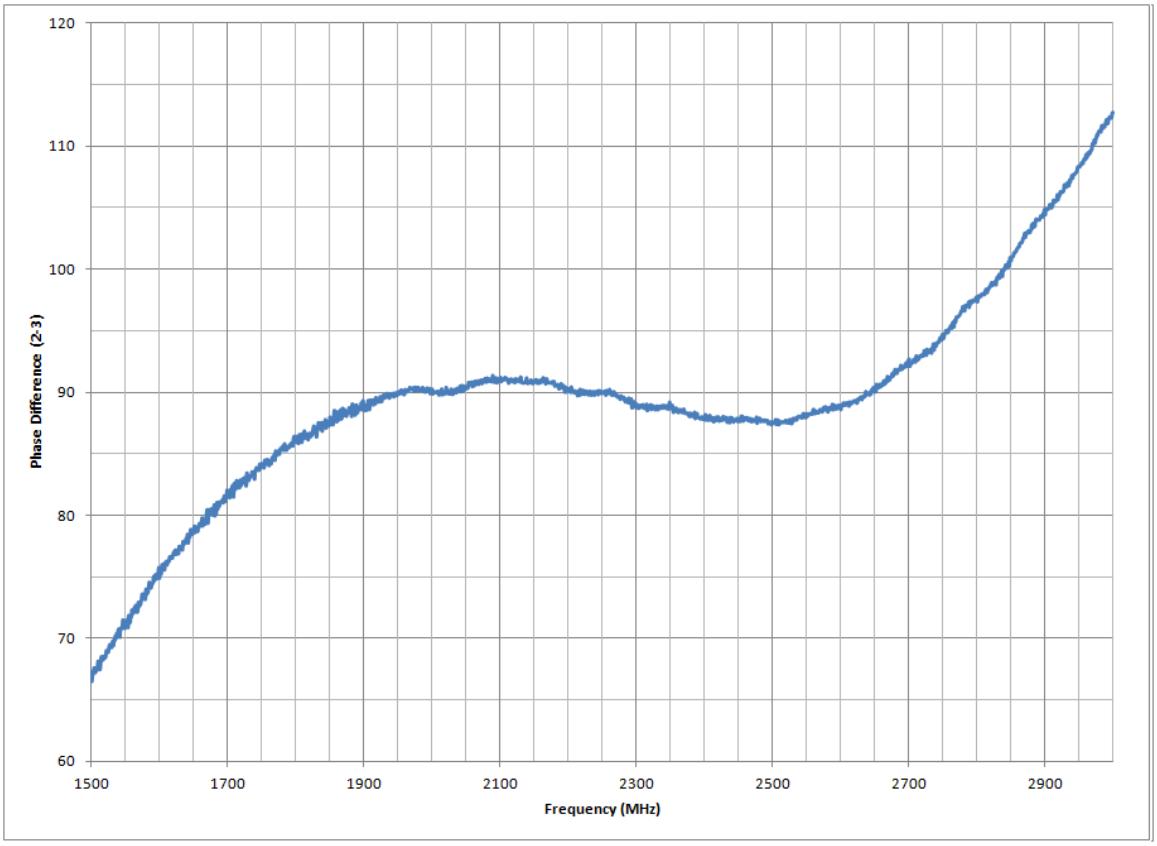

Figure 3.23: Design 2 Phase Difference

3.3.4 Discussion of Results

The second iteration of the hybrid coupler was much better than the original construction. Despite not operating at the desired center frequency of 1800 MHz, the device does behave as intended at its operating frequency of 2100 MHz. This is mostly likely due to the routing of the board. The depth of the end mill for the router is set by hand. Due to this, the mill cut into the substrate a small amount which would lower the effective dielectric constant of the microstrip; a lower effective

dielectric constant would cause the lengths of the quarter-wavelength sections to be a quarter-wavelength at a higher frequency. The device is well matched to 50 Ω at this frequency, provides good isolation, has a fairly even power split and has a large bandwidth where the phase difference between the output ports is 90°.

CHAPTER 4

Phase Shifter

This chapter will describe the simulation, design, construction and testing of the hybrid coupler phase shifter.

4.1 Design Goals

The goal for this phase shifter build is to provide a switched 90° phase shift (± 10 degrees) over a 5% bandwidth with less than 1 dB of insertion loss across the band. The shifter will be based on the second hybrid coupler build and therefore will ideally have a center frequency of approximately 2000 MHz.

4.2 Hybrid Coupler Phase Shifter

4.2.1 Design

The phase shifter design will be based on (2.14). In order to get a 90° phase shift, the stubs on ports 2 and 3 must be $\lambda_g/8$ long [8]. This can be found using

$$\Delta\phi = 4\pi\Delta l \tag{4.1}$$

where $\Delta\phi$ is the desired phase shift and Δl is the switched stub length in wavelengths.

4.2.2 Simulation

The design of the stub lengths was simulated in RF Sim to verify that the length provided the proper phase shift over the correct bandwidth as defined in the Design Goals. The simulation circuit is shown in figure 4.1 a and b. Figure 4.1a is the 90 degree shifted state and 4.1b is the 0 degree shifted state.

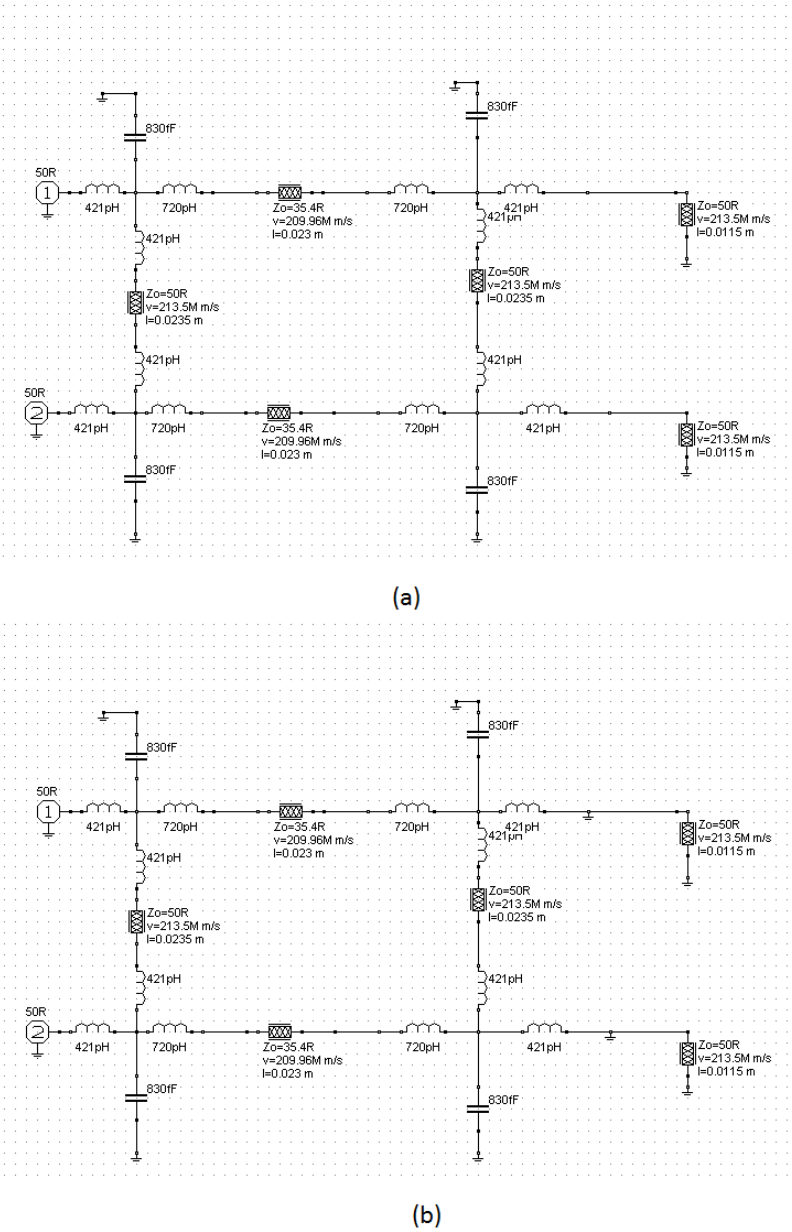

Figure 4.1: Phase Shifter Simulation Circuit

Using the circuit in figure 4.1, the phase shift of the circuit can be determined. The shift from this circuit is shown in figure 4.2. There are additional

markers placed at the 90°±10 degree locations within the 5% bandwidth to show the desired performance range.

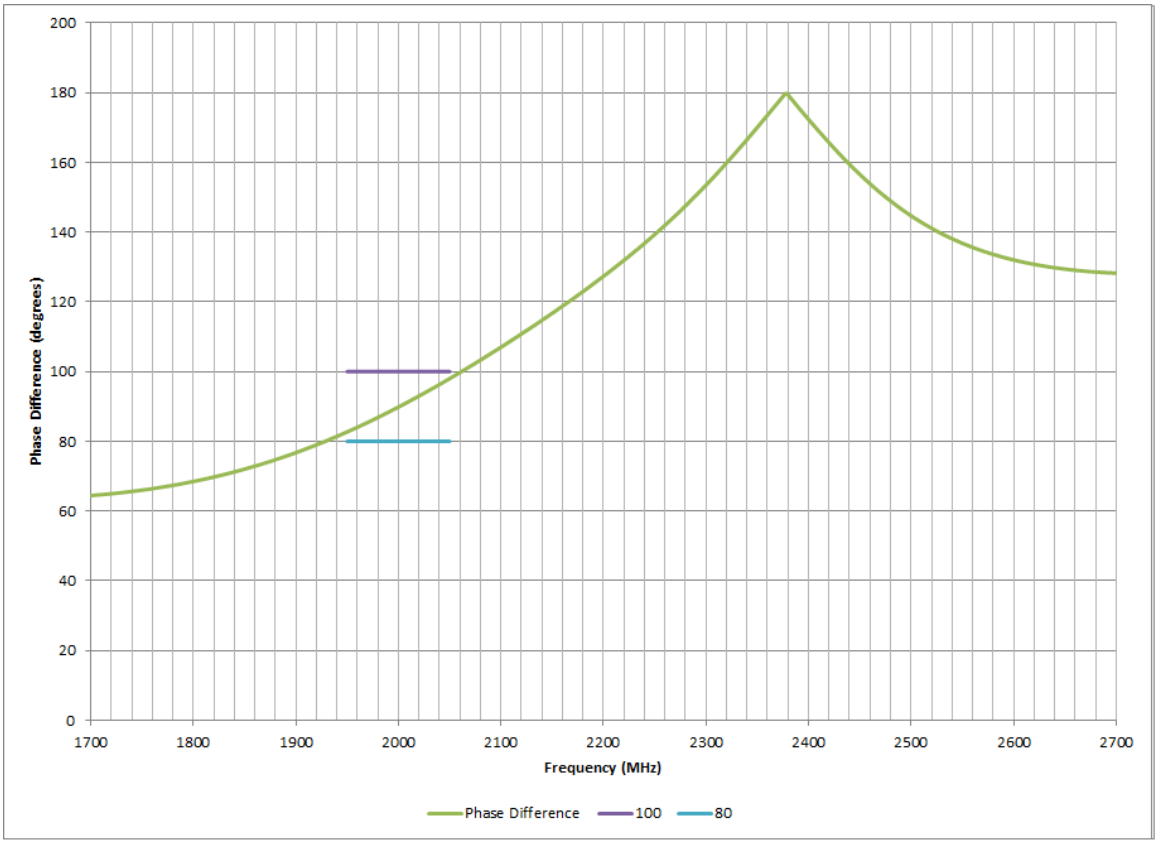

Figure 4.2: Phase Shifter Simulation Phase Shift

The phase shifter provides a 90°± 10 degrees over approximately a 5 % bandwidth. This matches the design goal for this shifter.

In addition to the phase shift the phase shifter provides, it should also have a reflection coefficient magnitude that is less than -10 dB over the operating band. The reflection coefficients of this circuit are shown in figure 4.3.

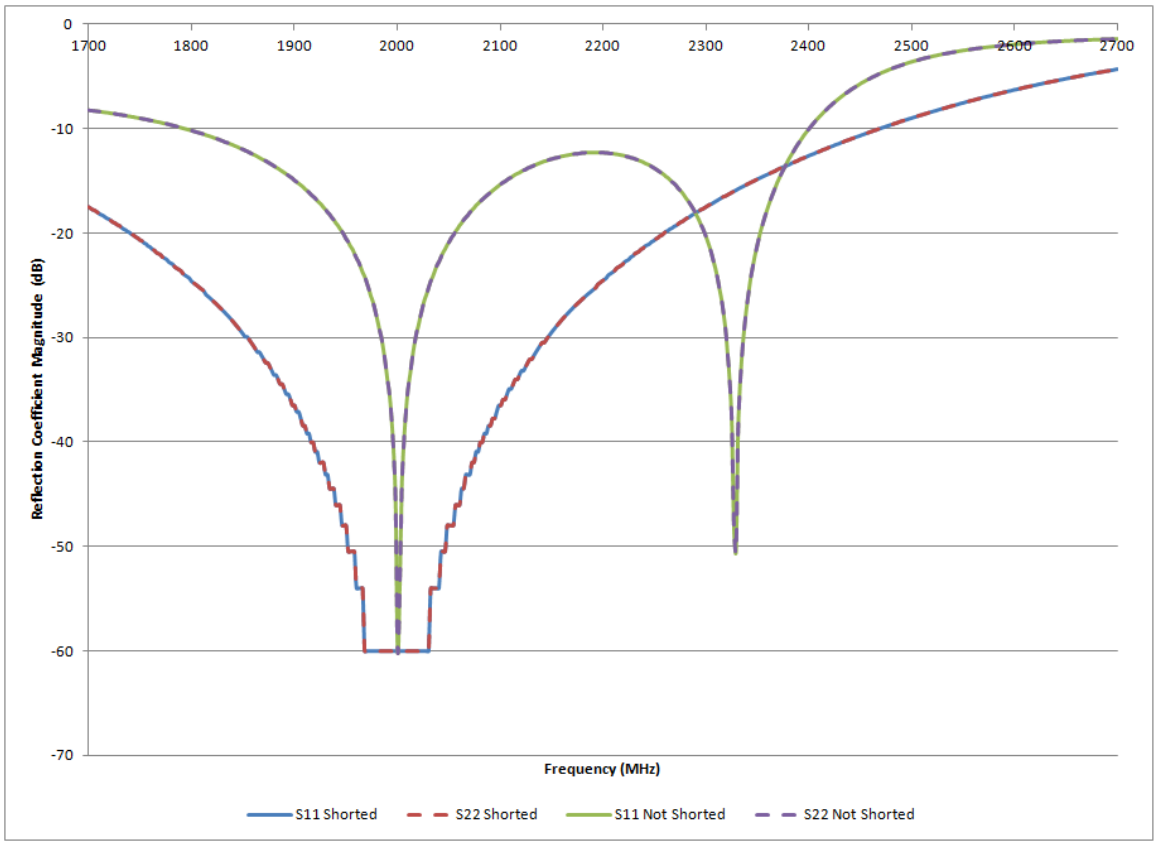

Figure 4.3: Phase Shifter Simulation Reflection Coefficient Magnitude

This circuit has a good match between 1800 and 2400 MHz where the reflection coefficient is below -10 dB for both states. This will provide good power transfer over the band of operation. (The steps in the simulation data are due to the software rounding to three decimal places.)

The phase shifter should also have a very low insertion loss in the operating band. This means the transmission coefficient magnitude should be above -1 dB. The transmission coefficient magnitudes of this circuit are shown in figure 4.4.

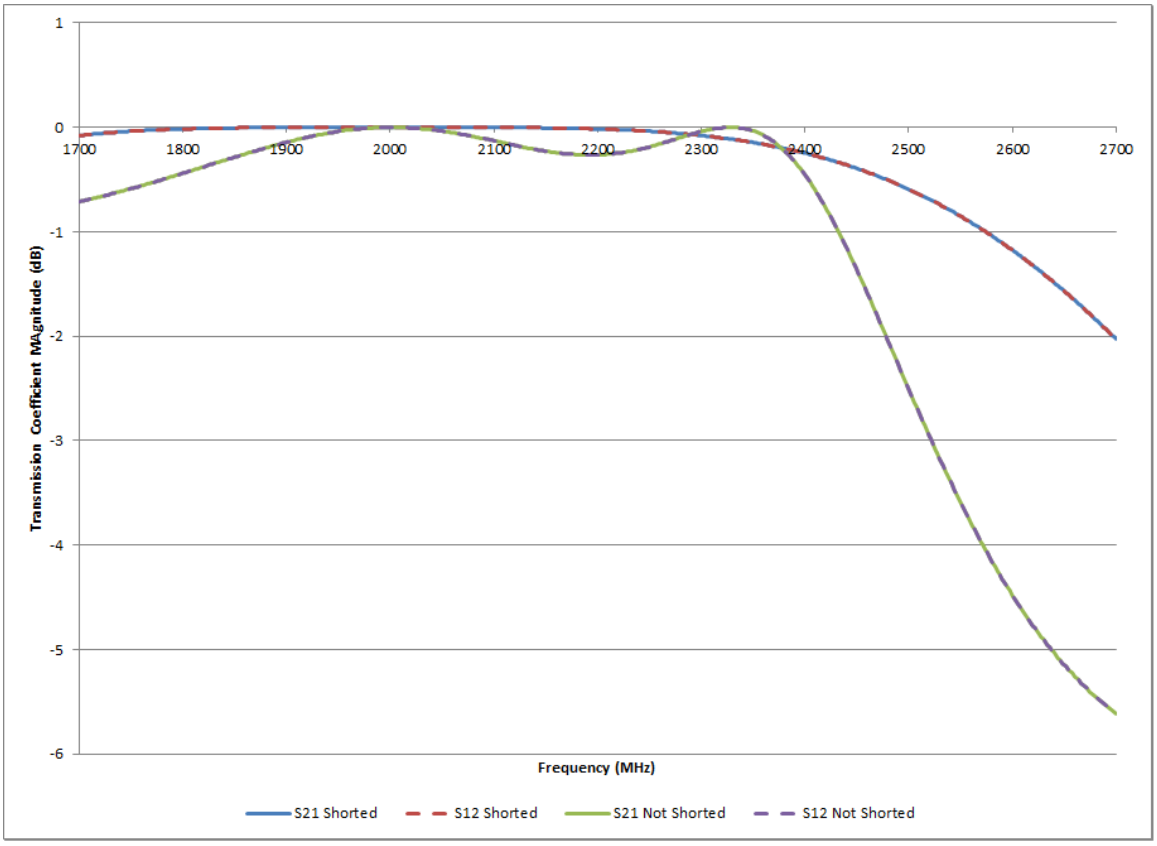

Figure 4.4: Phase Shifter Simulation Transmission Coefficient Magnitude

The transmission coefficient magnitudes are relatively low and are greater than -1 dB up to 2400 MHz which means that there is little loss through the device within the operating band.

The simulation parameters indicate that this device will provide a near 90° phase shift with low attenuation through the device in a 5% bandwidth centered at 2000 MHz which meets the design goals for this phase shifter.

4.2.3 Construction

In order to construct the phase shifter, the hybrid coupler from chapter 3 was built with extended traces on ports 2 and 3. The board was then cut to the appropriate length. Switching will be performed manually by applying copper tape which will short the traces to ground at a distance of $\lambda/8$ from the end of the stub. This is shown in figures 4.5 (0° phase shift) and 4.6 (90° phase shift).

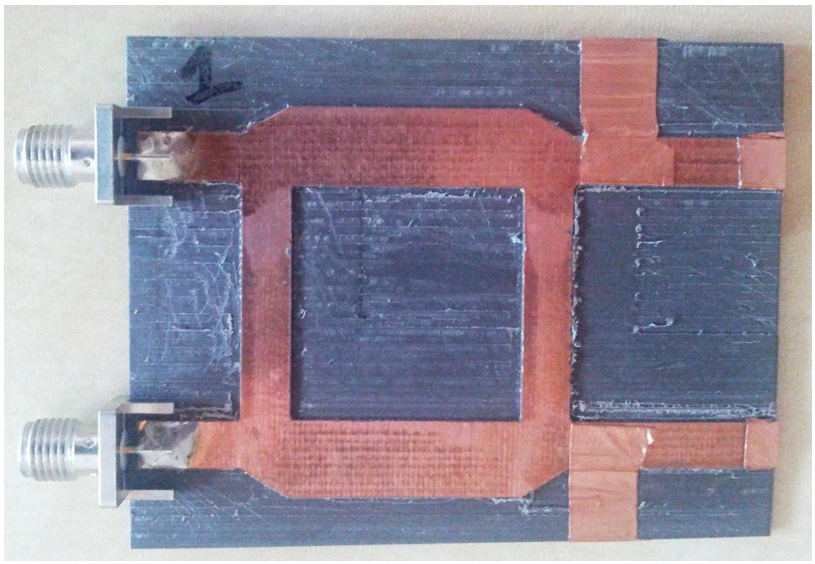

Figure 4.5: Phase Shifter Build with Short Traces (Also referred to as Shorted state)

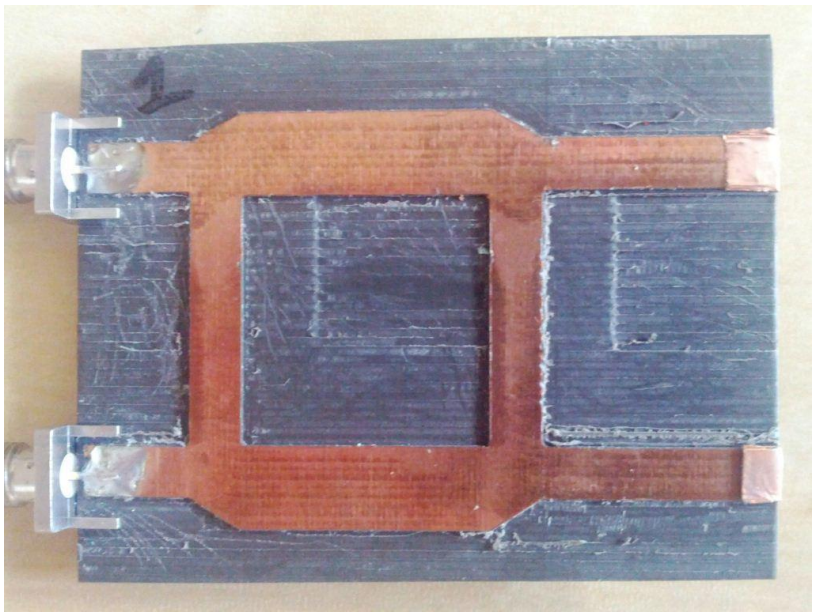

Figure 4.6: Phase Shifter Build with Long Traces (Also referred to as Not Shorted State)

4.2.4 Testing

The phase shifter was tested using a similar method used to test the hybrid coupler builds. In order to test the phase shifter performance of the device, two sets of measurements were needed for each of the shifter states.

Figure 4.7 shows the reflection coefficients for both states of the shifter.

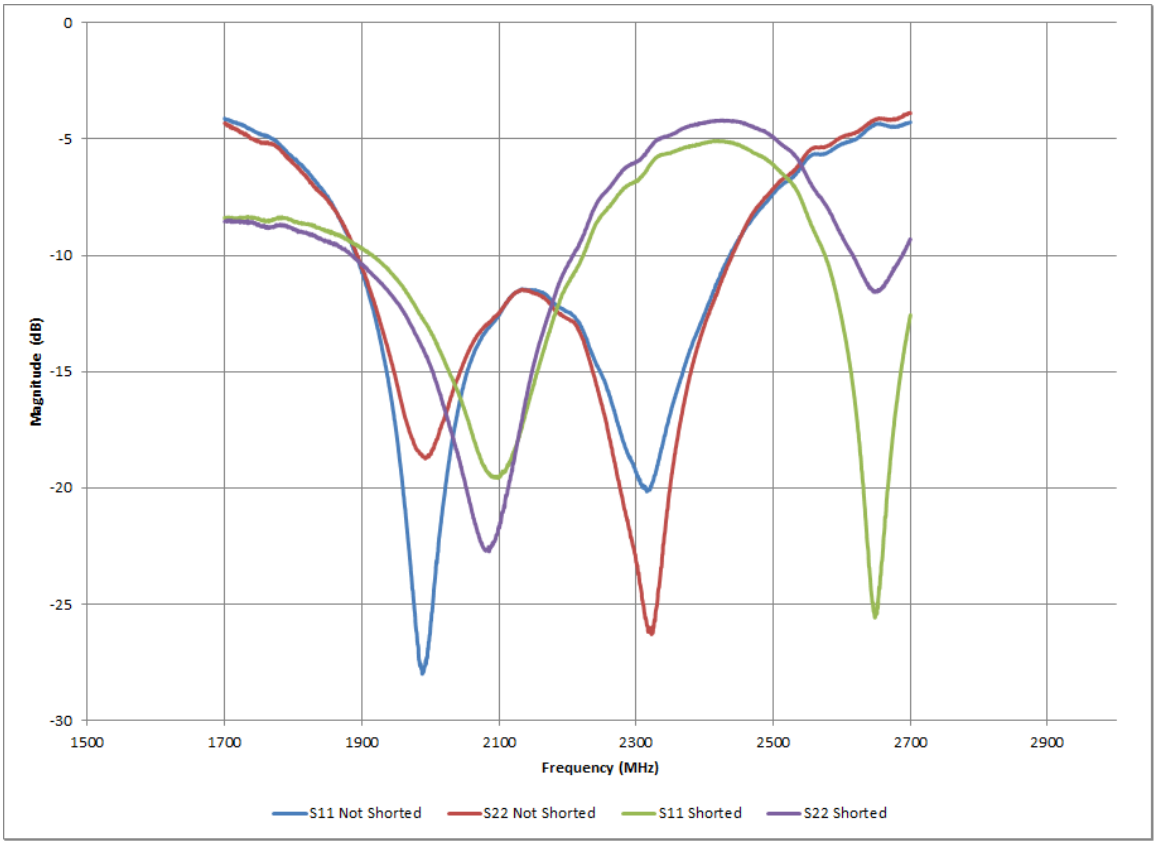

Figure 4.7: Phase Shifter Reflection Coefficient Magnitudes

The goal for this design was to have a reflection coefficient of less than -10 dB. Based on this specification, the device has a bandwidth of approximately 280 MHz (1920 to 2200 MHz). This exceeds the desired 100 MHz bandwidth of the design. These numbers differ from the simulated values due to losses in the system that are not accounted for in simulation.

Figures 4.8 and 4.9 show the transmission coefficients for both states of the shifter. The goal for this build was to have less than 1 dB of insertion loss across the band.

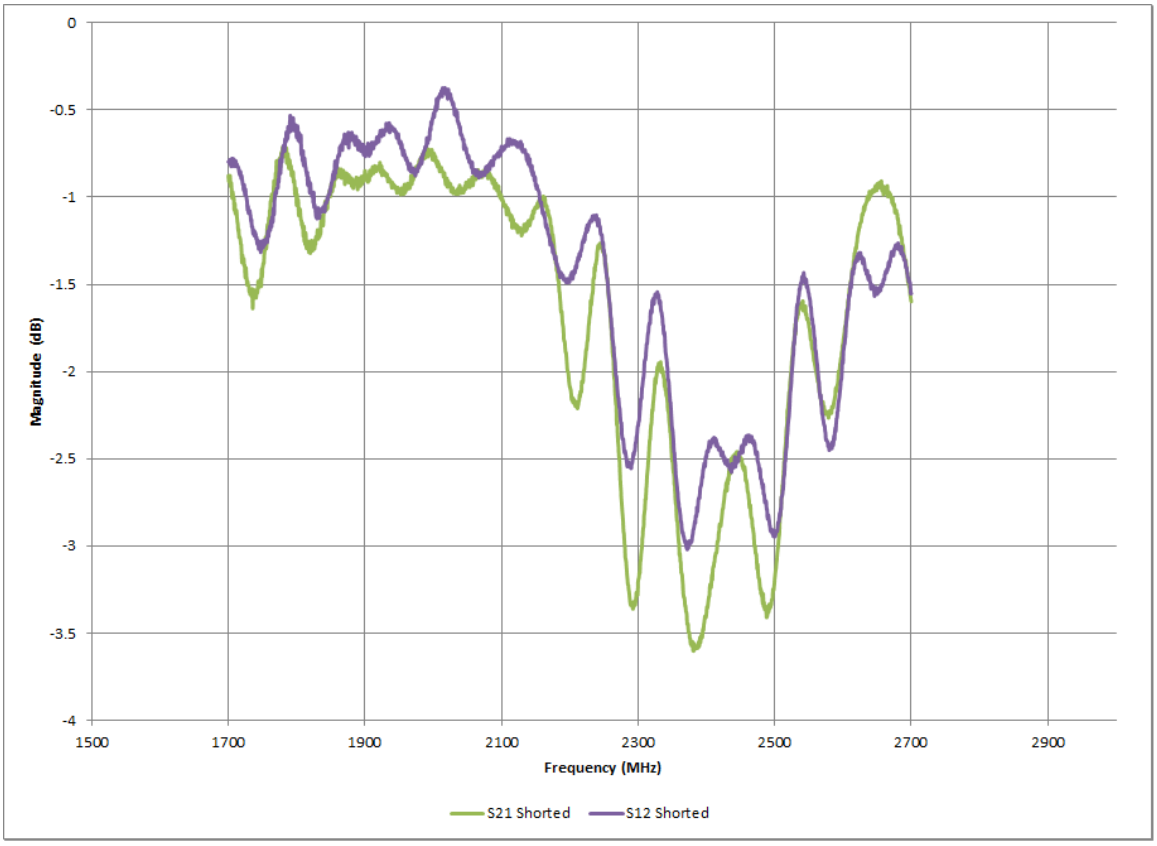

Figure 4.8: Phase Shifter Transmission Coefficient Magnitude (Shorted State)

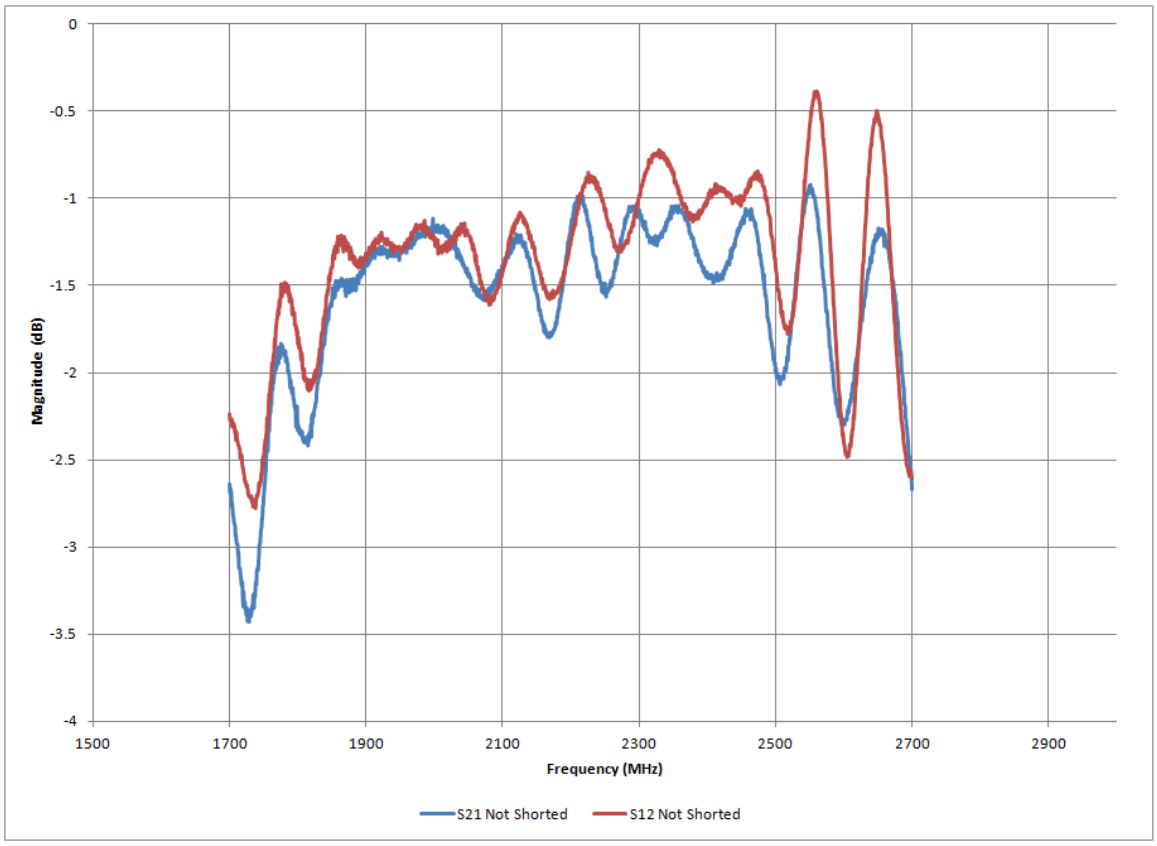

Figure 4.9: Phase Shifter Transmission Coefficient Magnitude (Not Shorted State)

These values do not fall below 1 dB of insertion loss over the desired band. There is some additional loss through the device due to resistive loss and dielectric loss tangent that is not accounted for by the simulation. There is also a large amount of variation in amplitude over frequency in the measurement. This variation is not a reflection of the actual device performance, but is rather due to errors in the calibration setup for the VNA. This effect is only present on amplitude measurements of through-port measurements and is most notable on lower loss devices like this phase shifter. Taking an average through the variation gives a

better metric of the actual performance. Using this technique, the phase shifter has an insertion loss of less than 1.5 dB over a wide bandwidth that covers much more than the band of interest.

Figure 4.10 shows the phase difference of the transmission coefficients for both states. The goal for this was a 90° (±10 degrees) phase shift.

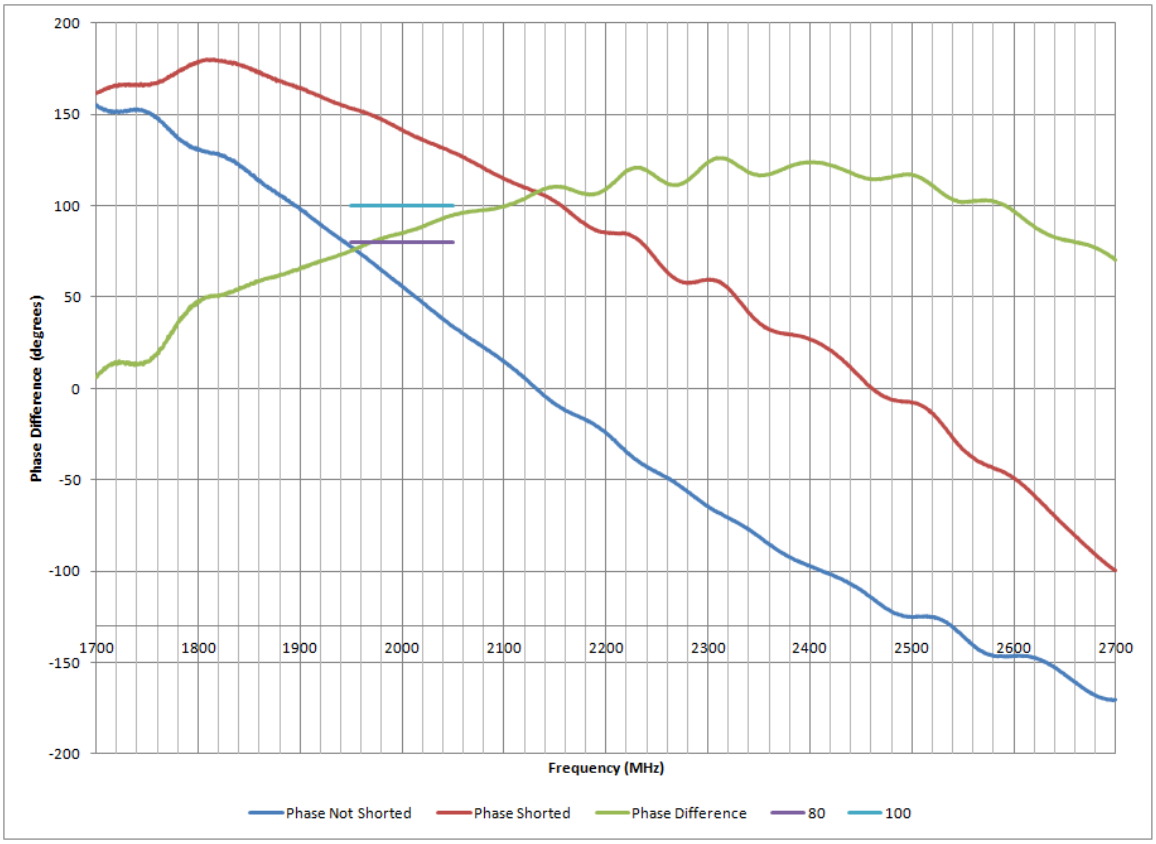

Figure 4.10: Phase Shifter Transmission Coefficient Phase Difference

Similarly to the hybrid coupler design, the phase response of the circuit did not meet the desired specifications. The design did not quite meet the 5% bandwidth at 2000 MHz. It was slightly shifted up in frequency from the expected

design. These measurements were made using non-phase stable cables which can introduce large variation in measurements due to small variations in cable bends or from cable movement during measurement. This could easily account for the small offset in measured results seen in figure 4.10.

4.2.5 Discussion of Results

This design did not meet the desired specifications. In addition to measurement equipment error, there was also likely error due to not including the additional effects of shorting the traces with a short transmission line instead of a using direct short in simulation. When compensating for these effects, the performance of the device is greatly improved. Simulation shows that a 90° phase shift can be achieved over a wider bandwidth by using a stub length of 0.018 meters.

Updated simulation results show that the 90 degree (±10 degree) bandwidth is approximately 220 MHz or 11% at 2000 MHz as shown in figure 4.11.

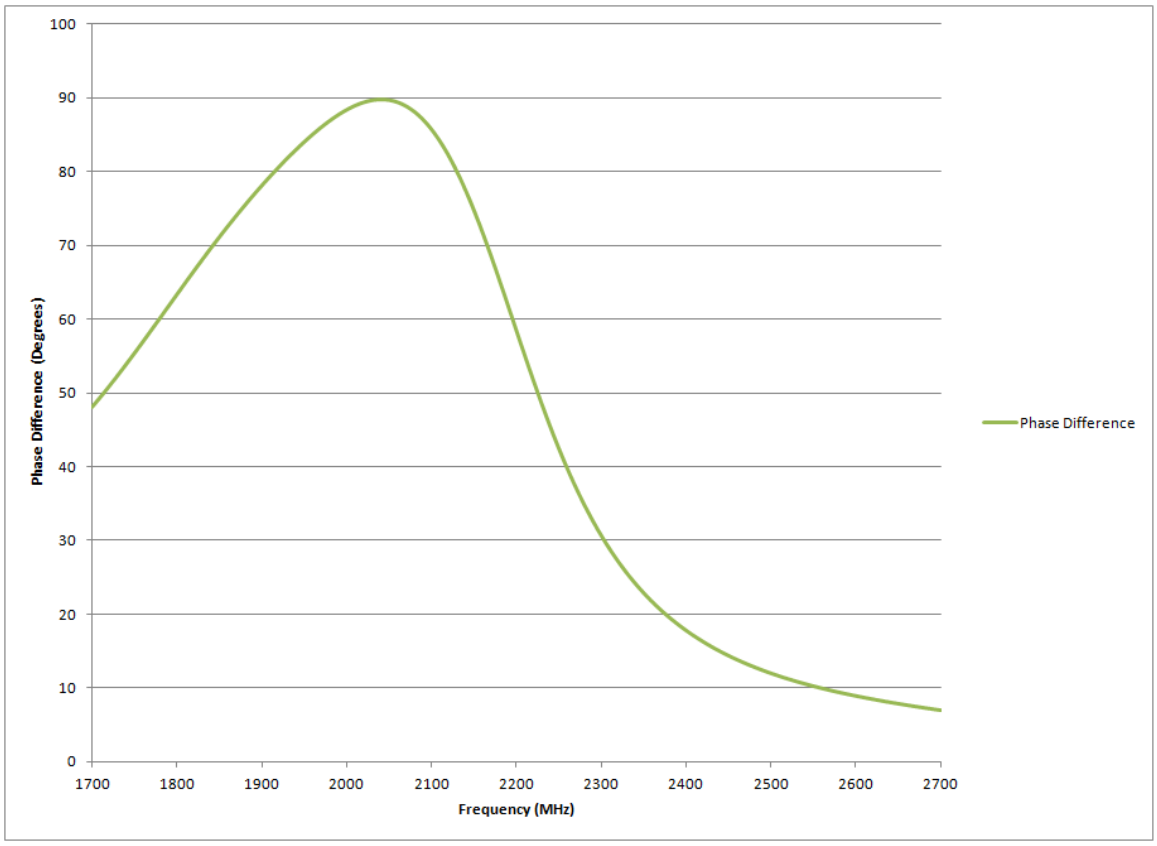

Figure 4.11: Updated Phase Shifter Simulation Phase Shift

Although there is improved phase response, this change gives a worse reflection coefficient performance over the band. The new reflection coefficients for this circuit can be seen in figure 4.12.

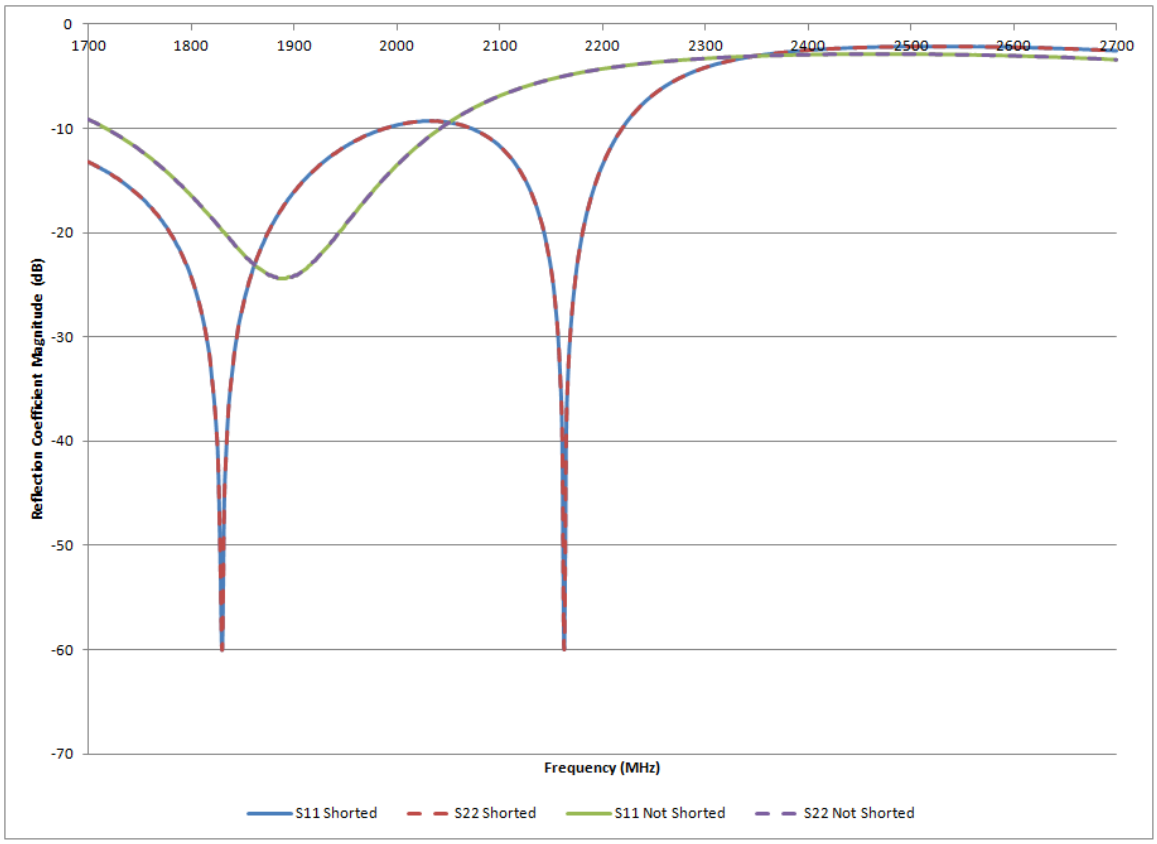

Figure 4.12: Updated Phase Shifter Simulation Reflection Coefficients

The reflection coefficient rises above -10 dB near the band of interest. However, the magnitude peaks near -9.3 dB which still will provide a fairly good match over this bandwidth.

There is also slight degradation of the transmission coefficient for the circuit which can be seen in figure 4.13.

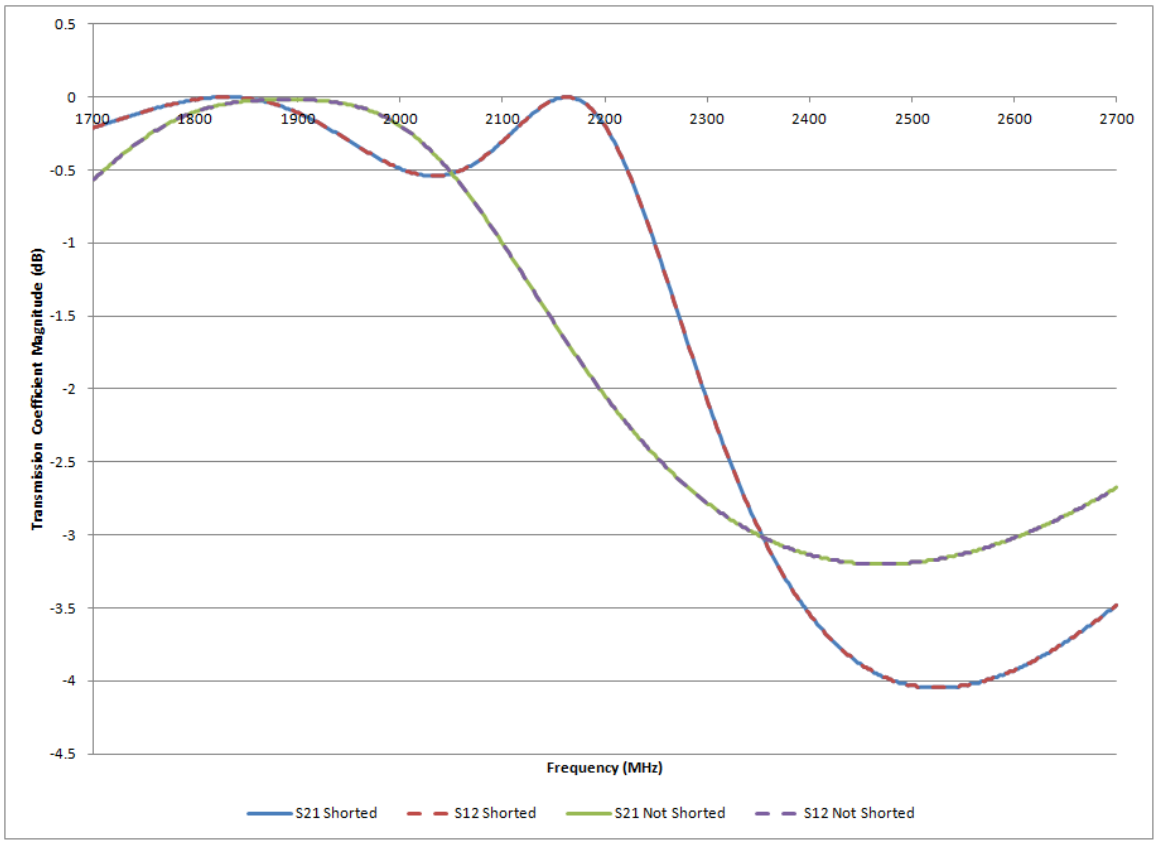

Figure 4.13: Updated Phase Shifter Simulation Transmission Coefficients

Although the transmission coefficients fall below -1 dB, they are still above -1.5 dB within the 5% bandwidth desired for the circuit which will provide low loss through the device that can be easily balanced with an equalizer.

Making these changes should allow for the construction of a phase shifter which will more closely meet the desired specifications as was seen with the second iteration of the hybrid coupler. However, this will not be pursued in this thesis.

CHAPTER 5

Conclusions

5.1 Conclusions

The goal for this work was to build a microstrip hybrid coupler centered at 1800 MHz and a hybrid coupler phase shifter which provides a 90° phase shift over a 5% bandwidth centered at 1800 MHz.

The results of the hybrid coupler builds were very promising. After the second iteration, the coupler had very good behavior with respect to power split and phase shift. However, these parameters were all shifted up in frequency, primarily due to poor construction techniques. This could be easily remedied in another build.

The results for the phase shifter build were further from the desired specifications. With time, another shifter could be built using the additional simulation results as well as improved construction and switching techniques that would more closely meet these specifications.

5.2 Lessons Learned

One of the biggest lessons learned during this work is that the analysis of microstrip based devices can be very complex. There are many parasitic effects which are present in microstrip circuits. These parasitics require additional simulation techniques in order to obtain accurate results. This is mostly due to the difficulty in finding accurate parasitic parameters to use in the simulation. The methods used in this work were rather rudimentary due to the lack of powerful simulation tools and relied on curve fit approximations to obtain estimates for junction parasitics.

In addition to complex simulation and analysis, microstrip devices also require precise manufacturing techniques in order to perform as intended. Small variations from cutting into the substrate too far or width changes from cutting inaccuracies can have a significant effect on the frequency behavior of the device. Great care must be taken to insure that the board and cuts are made precisely in order to obtain the desired results from the device.

5.3 Suggestions for Future Work

The main purpose of this thesis was to present analysis and simulation of a hybrid coupler phase shifter. The analysis work was thoroughly completed, but the

simulation was performed with relatively basic software that was available. With access to a more robust simulation package, better approximations for the behavior of the microstrip traces and junctions could be found. This would provide a better design once constructed. The software package may also allow for simulation of the phase shifter to be performed with measured S-parameter results of the hybrid coupler. With this type of simulation, the phase shifter design could be optimized to work with the specific hybrid coupler that was constructed for this work.

In addition to improving the simulation, the construction of the device could be improved. Cutting the copper with the board router removed some of the substrate as well. This caused the frequency performance of the device to shift upwards. With additional resources and time, the microstrip traces that comprise the device could have been cut more precisely or etched out of a copper layer to preserve the proper height of the substrate and preserve the desired frequency performance of the circuit.

For this project, only one device was constructed for each iteration of the coupler and for the phase shifter. An investigation into the repeatability of the design could be performed. This would further validate the design and provide a measure of quality for the fabrication techniques used in this work.

Additionally, a switching circuit or mechanism could have been devised in place of simply applying copper traces to short the stubs. This would provide more

stable performance since the switching would be more repeatable and would not mechanically stress the copper traces used to switch the phase in the current design. Several design choices could be used including mechanical switches or PIN diode switches. This would require additional simulation in order to account for the effects of the switching mechanism used.

Another phase shifter device could be constructed based on updated simulation to obtain results that would be more in line with the desired specifications as was done for the hybrid couplers. This would allow for verification of the updated simulation data and provide a more useful shifter for use in a system like a phased antenna array.

Lastly, this phase shifter could be implemented into a phased antenna array system. This would test the performance and quality of the shifter when used in a full system.

BIBLIOGRAPHY

[1] J.F. White, "Diode phase shifters for array antennas", *Microwave Theory and Techniques, IEEE Transactions on*, vol. 22, no. 6, pp. 658 – 674, Jun 1974.

[2] David M. Pozar, *Microwave Engineering*, John Wiley and Sons, Inc., Hoboken, NJ, 3rd edition, 2005.

[3] Shiban K. Koul and Bharathi Bhat, *Microwave and Millimeter Wave Phase Shifters*, vol. I and II, Artech House, Norwood, MA, 1991.

[4] Joseph Helszajn, *Ferrite Phase Shifters and Control Devices*, Mcgraw Hill, TX, 1989.

[5] "PIN diode designers handbook", `http://www.ieee.li/pdf/pin_diode_handbook.pdf`, Microsemi, Accessed January, 2012.

[6] Robert J. Weber, *Introduction to Microwave Circuits*, IEEE Press, Piscataway, NJ, 2001.

[7] "Microwave power dividers and couplers tutorial", `http://www.markimicrowave.com/menus/appnotes/Microwave_Power_Dividers_and_Couplers_Primer.pdf`, Marki Microwave, Accessed January, 2012.

[8] R.V. Garver, "Broadband diode phase shifters", *Microwave Symposium Digest, 1971 IEEE GMTT International*, pp. 178 –179, May 1971.

[9] J. Reed and G.J. Wheeler, "A method of analysis of symmetrical four-port networks", *Microwave Theory and Techniques, IRE Transactions on*, vol. 4, no. 4, pp. 246 –252, October 1956.

[10] "RT duroid 5870/5880 datasheet", `http://www.rogerscorp.com/documents/606/acm/RT-duroid-5870-5880-Data-Sheet.aspx`, Rogers Corporation, Accessed March, 2012.

[11] T.C. Edwards, *Foundations of interconnect and microstrip design*, John Wiley, Chichester, West Sussex, England, 3rd edition, 2000.

[12] "LPKF protomat c40 datasheet", `http://www.lpkfusa.com/datasheets/prototyping/plotter.pdf`, LPKF, Accessed March, 2012.

[13] Kenneth E. Mortenson, *Variable Capacitance Diodes*, Artech House, Dedham, MA, 1974.

[14] J.P. Starski, "Optimization of the matching network for a hybrid coupler phase shifter", *Microwave Theory and Techniques, IEEE Transactions on*, vol. 25, no. 8, pp. 662 – 666, Aug 1977.

[15] M.H. Kori and S. Mahapatra, "Integral analysis off hybrid coupled semiconductor phase shifters", *Microwaves, Antennas and Propagation, IEE Proceedings H*, vol. 134, no. 2, pp. 156 –162, April 1987.

[16] "Width and effective dielectric constant equations for design of microstrip transmission lines", `http://www.rogerscorp.com/documents/780/acm/Design-Data-for-Microstip-Transmission-Lines-on-RT-duroid-Laminates.aspx`, Rogers Corporation, Accessed February, 2012.

[17] T.G. Bryant and J.A. Weiss, "Parameters of microstrip transmission lines and of coupled pairs of microstrip lines", *Microwave Theory and Techniques, IEEE Transactions on*, vol. 16, no. 12, pp. 1021 – 1027, Dec 1968.

[18] E. Hammerstad and O. Jensen, "Accurate models for microstrip computer-aided design", in *Microwave symposium Digest, 1980 IEEE MTT-S International*, May 1980, pp. 407 –409.

[19] Constantine A. Balanis, *Advanced Engineering Electromagnetics*, John Wiley and Sons, Inc., Hoboken, NJ, 2nd edition, 2012.

[20] P. Silvester and P. Benedek, "Microstrip discontinuity capacitances for right-angle bends, t junctions, and crossings", *Microwave Theory and Techniques, IEEE Transactions on*, vol. 21, no. 5, pp. 341 – 346, may 1973.

APPENDIX A

Transmission (ABCD) Matrices

The transmission, or ABCD, matrix is a 2 x 2 matrix which relates the voltages and currents of a two-port device. It is very useful because it provides a method of easily cascading two-port networks and finding the total response of the system. This becomes very useful in many microwave systems (e.g. filters, amplifiers, series/shunt components and transmission line sections) as they tend to be a cascade of several two-port networks [2].

A.1 Transmission Matrix Definition

The voltages and currents for the ABCD matrix are shown in figure A.1.

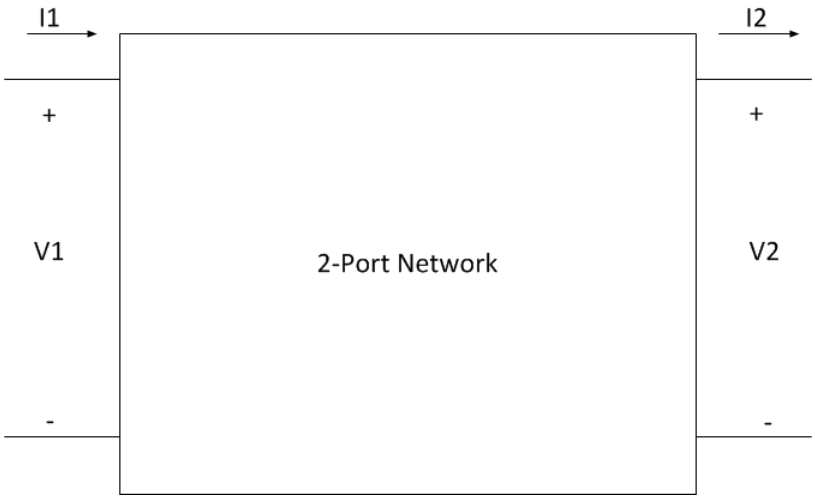

Figure A.1: ABCD Two-Port Network Voltage and Current Definitions

These voltages and currents can be related by

$$V_1 = AV_2 + BI_2 \tag{A.1a}$$

$$I_1 = CV_2 + DI_2 \tag{A.1b}$$

where V_1 is the total voltage at port 1, I_1 is the net current entering port 1, V_2 is the total voltage at port 2, I_2 is the net current leaving port 2 and $A, B, C,$ and D are the elements of the ABCD matrix which relate the voltages and currents. These elements can be defined as

$$A = \left.\frac{V_1}{V_2}\right|_{I_2=0} \tag{A.2a}$$

$$B = \left.\frac{V_1}{I_2}\right|_{V_2=0} \tag{A.2b}$$

$$C = \left.\frac{I_1}{V_2}\right|_{I_2=0} \tag{A.2c}$$

$$D = \left.\frac{I_1}{I_2}\right|_{V_2=0} \tag{A.2d}$$

Eqn. A.1 can be rewritten in matrix form as

$$\begin{bmatrix} V_1 \\ I_1 \end{bmatrix} = \begin{bmatrix} A & B \\ C & D \end{bmatrix} \begin{bmatrix} V_2 \\ I_2 \end{bmatrix} \tag{A.3}$$

A.2 Cascading Transmission Matrices

If two or more two-port networks are cascaded in series, the total response of the system can be found by multiplying the ABCD matrices together. This can be shown by analyzing the circuit in figure A.2.

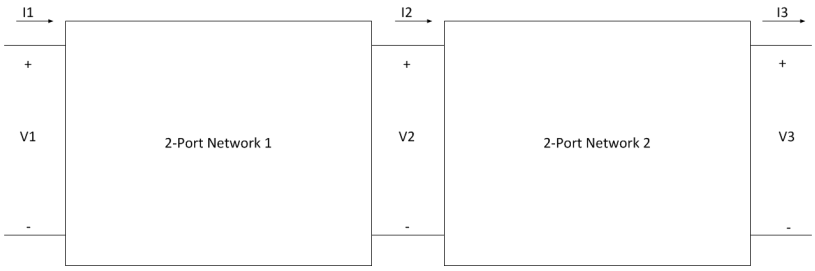

Figure A.2: ABCD Two-Port Network Cascade Voltage and Current Definitions

Since both networks are two-port networks, they can be characterized by their ABCD matrices as

$$\begin{bmatrix} V_1 \\ I_1 \end{bmatrix} = \begin{bmatrix} A_1 & B_1 \\ C_1 & D_1 \end{bmatrix} \begin{bmatrix} V_2 \\ I_2 \end{bmatrix} \tag{A.4}$$

$$\begin{bmatrix} V_2 \\ I_2 \end{bmatrix} = \begin{bmatrix} A_2 & B_2 \\ C_2 & D_2 \end{bmatrix} \begin{bmatrix} V_3 \\ I_3 \end{bmatrix} \tag{A.5}$$

By substitution, the final response of the system can be written as

$$\begin{bmatrix} V_1 \\ I_1 \end{bmatrix} = \begin{bmatrix} A_1 & B_1 \\ C_1 & D_1 \end{bmatrix} \begin{bmatrix} A_2 & B_2 \\ C_2 & D_2 \end{bmatrix} \begin{bmatrix} V_3 \\ I_3 \end{bmatrix} \tag{A.6}$$

Eqn. A.6 shows that the total ABCD matrix for the system is simply the product of the individual elements. Note that this multiplication must take place in the order that the individual networks appear in the cascade.

A.3 Conversion to S Matrix

Once the total response of the system is known, it is often convenient to convert this result back to the S matrix for further analysis of the system. This can be accomplished by using

$$S_{11} = \frac{A + B/Z_0 - CZ_0 - D}{A + B/Z_0 + CZ_0 + D} \tag{A.7a}$$

$$S_{21} = \frac{2(AD - BC)}{A + B/Z_0 + CZ_0 + D} \tag{A.7b}$$

$$S_{12} = \frac{2}{A + B/Z_0 + CZ_0 + D} \tag{A.7c}$$

$$S_{22} = \frac{-A + B/Z_0 - CZ_0 + D}{A + B/Z_0 + CZ_0 + D} \tag{A.7d}$$

where Z_0 is the characteristic impedance of the network [2].

APPENDIX B

Effective Dielectric Constants in Microstrip

B.1 Microstrip Geometry

Microstrip line is a planar transmission line which consists of a conductor trace on top of a dielectric substrate. The bottom side of the dielectric substrate is covered with a conducting ground plane. The basic geometry of a microstrip trace is shown in figure B.1.

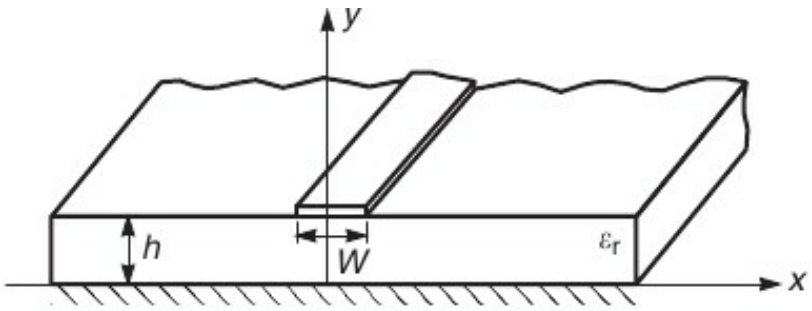

Figure B.1: Microstrip Trace Geometry [2]

The approximate field lines for this structure are shown in figure B.2.

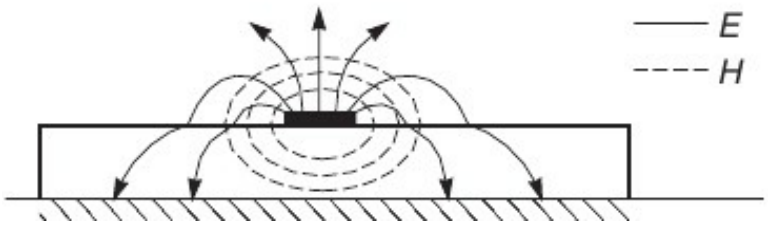

Figure B.2: Approximate Microstrip Field Lines [2]

B.2 Effective Dielectric Constant

Because some of the fields exist in the dielectric and some exist in the air, the structure cannot support a true TEM wave. However, in practical applications, when the substrate is much smaller than a wavelength, a quasi-TEM mode exists (i.e. the fields in the cross-section behave approximately like the static case). Using static results, approximations for phase velocity and propagation constant can be written as

$$v_{ph} = \frac{c}{\sqrt{\epsilon_e}} \tag{B.1a}$$

$$\beta = k_0\sqrt{\epsilon_e} \tag{B.1b}$$

where k_0 is the free space propagation constant, v_{ph} is the phase velocity, and ϵ_e is the effective dielectric constant. These equations both assume that the material is non-magnetic (i.e. μ is equal to μ_0). The effective dielectric constant accounts for

some of the fields being in the air and the rest being in the dielectric substrate. Its value is between 1 (the relative dielectric constant for air) and ϵ_r (the dielectric constant of the substrate). The effective dielectric constant is a function of the height of the substrate and the width of the conductor [2]. For typical transmission line structures at frequencies below approximately 2.5 GHz, the effective dielectric constant has negligible variation due to frequency. For frequencies above this, the constant is strongly affected by frequency [19]. The approximation for ϵ_e at low frequency is given as

$$\epsilon_e = \frac{\epsilon_r + 1}{2} + \frac{\epsilon_r - 1}{2} \frac{1}{\sqrt{1 + 12d/W}} \tag{B.2}$$

where d is the height of the substrate and W is the width of the conducting strip.

The ratio of W/d can be found for a given characteristic impedance, Z_0, and a relative dielectric constant to be

$$\frac{W}{d} = \begin{cases} \frac{8e^A}{e^{2A}-2} \\ \frac{2}{\pi}\left[B - 1 - \ln(2B-1) + \frac{\epsilon_r - 1}{2\epsilon_r}\right]\left[\ln(B-1) + 0.39 - \frac{0.61}{\epsilon_r}\right] \end{cases} \tag{B.3}$$

where

$$A = \frac{Z_0}{60}\sqrt{\frac{\epsilon_r + 1}{2}} + \frac{\epsilon_r - 1}{\epsilon_r + 1}\left(0.23 + \frac{0.11}{\epsilon_r}\right) \tag{B.4a}$$

$$B = \frac{377\pi}{2Z_0\sqrt{\epsilon_r}} \tag{B.4b}$$

Eqns. B.3 and B.4 are based on curve fit approximations [2].

APPENDIX C

Junction Parasitics for Microstrip T-Junctions

The microstrip T-junction is very common in microstrip circuits. The basic layout of a T-junction is shown in figure C.1.

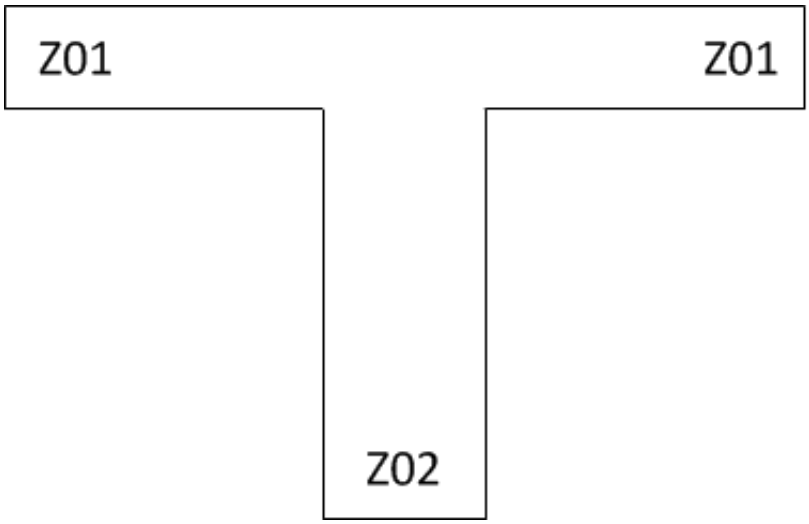

Figure C.1: T-Junction Microstrip Layout

The right angle bends and step discontinuities in the structure require that parasitic capacitance and inductance be included in modeling this junction. In addition, there is also a transformer that must be included in the shunt microstrip branch [11]. The equivalent circuit for the T-junction is shown in figure C.2.

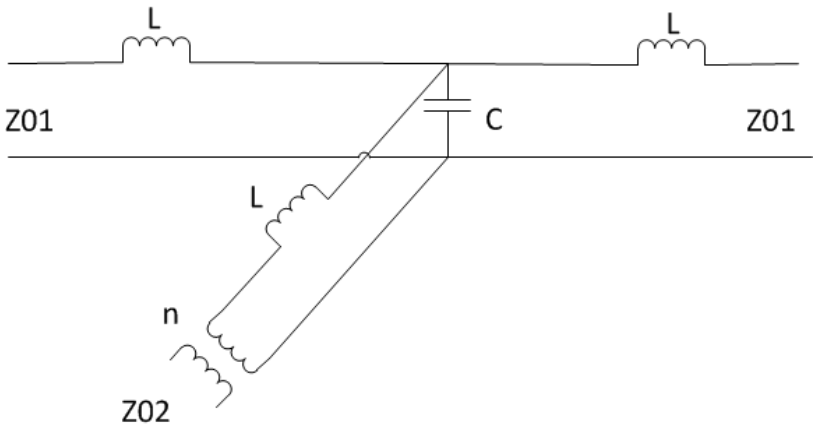

Figure C.2: T-Junction Equivalent Circuit

C.1 Junction Parasitic Calculations

In order to use these models in simulation, the capacitance, inductance and transformation ratio need to be calculated. These values have been experimentally and theoretically calculated by several authors [11].

The transformation ratio, n is given by

$$n = \left[\frac{\sin(\pi(w_{eff1}/\lambda_{g1})(Z_{01}/Z_{02}))}{\pi(w_{eff1}/\lambda_{g1})(Z_{01}/Z_{02})}\right][1 - \pi(w_{eff1}/\lambda_{g1})(d_2/w_{eff1})] \tag{C.1}$$

where Z_0 is the characteristic impedance, λ_{g1} is the wavelength in the microstrip for the microstrip with characteristic impedance Z_{01}, the effective width of the microstrip is given by

$$w_{eff} = \frac{h\eta}{Z_0\sqrt{\epsilon_{eff}}} \tag{C.2}$$

where h is the height, η is the free space wave impedance and

$$\frac{d_2}{w_{eff1}} = 0.5 - \left[0.076 + 0.2\left(\frac{2w_{eff1}}{\lambda_{g1}}\right)^2 + 0.663\exp\left(-1.71\frac{Z_{01}}{Z_{02}}\right) - 0.172\ln\left(\frac{Z_{01}}{Z_{02}}\right)\right]\frac{Z_{01}}{Z_{02}} \tag{C.3}$$

The shunt capacitance value, C, can be found using

$$\frac{\omega C\lambda_{g1}}{Y_{01}w_{eff1}} = \left(\frac{2w_{eff1}}{\lambda_{g1}} - 1\right)\left(2 - 3\frac{Z_{01}}{Z_{02}}\right) \tag{C.4}$$

where ω is the center frequency and Y_0 is the characteristic admittance. This equation holds true while

$$\frac{Z_{01}}{Z_{02}} > 0.5 \tag{C.5}$$

The values for T-junction parasitic inductance used in this paper were approximated to be near the same value as the right angle junction. The inductance (in nH) can be found using

$$L = 100\left[4 * \sqrt{\frac{w}{h}} - 4.21\right]h \tag{C.6}$$

where w is the strip width and h is the height of the substrate.